Analyse du rayonnement UVB pendant les événements d'influence du trou d'ozone antartique sur le sud du Brésil

Bibiana Culau Lopes

▶ **To cite this version:**

Bibiana Culau Lopes. Analyse du rayonnement UVB pendant les événements d'influence du trou d'ozone antartique sur le sud du Brésil. Physique Atmosphérique et Océanique [physics.ao-ph]. Université de la Réunion; Universidade federal de Santa Maria (Brésil), 2022. Français. NNT : 2022LARE0009 . tel-03771818

HAL Id: tel-03771818
https://theses.hal.science/tel-03771818

Submitted on 7 Sep 2022

HAL is a multi-disciplinary open access archive for the deposit and dissemination of scientific research documents, whether they are published or not. The documents may come from teaching and research institutions in France or abroad, or from public or private research centers.

L'archive ouverte pluridisciplinaire **HAL**, est destinée au dépôt et à la diffusion de documents scientifiques de niveau recherche, publiés ou non, émanant des établissements d'enseignement et de recherche français ou étrangers, des laboratoires publics ou privés.

Analysis of the UVB radiation during the events of influence of the Antarctic ozone hole over south of Brazil

By

Bibiana Culau Lopes

Submitted in fulfillment of the requirements for the degree Doctor in Meteorology in the Graduate Program in Meteorology, Federal University of Santa Maria

Supervisor: Dr. Damaris Kirsch Pinheiro

And

Docteur és Sciences (Physique de l'atmosphere)
Sciences Technologies Santé (ED542), Physique de l'Atmosphère,
Laboratoire de l'Atmosphère et des Cyclones – LACy UMR 8105
Université de La Réunion

Supervisor: Dr. Hassan Bencherif

Members of the jury:

Thierry Portafaix, Dr. (UR)
Lucas Vaz Peres, Dr. (UR)
Luiz Angelo Steffenel, Dr. (URCA)
Everson Dal Piva, Dr. (UFSM)
Vagner Anabor, Dr. (UFSM)

13 June 2022

Bibiana Culau Lopes

ANALYSIS OF THE UVB RADIATION DURING THE EVENTS OF INFLUENCE OF THE ANTARCTIC OZONE HOLE OVER SOUTH OF BRAZIL

Tese de Tese de Doutorado apresentada ao programa de Pós-Graduação em Meteorologia, Área de Concentração em Estudos e Aplicações em Tempo e Clima, da Universidade Federal de Santa Maria (UFSM, RS), como requisito parcial para obtenção do grau de **Doutora em Meteorologia**.

Aprovado em 13 de junho de 2022:

Damaris Kirsch Pinheiro, Dra. (UFSM)
(Presidenta/Orientadora)

Hassan Bencherif, Dr. (UR)

Thierry Portafaix, Dr. (UR)

Lucas Vaz Peres, Dr. (UR)

Luiz Angelo Steffenel, Dr. (URCA)

Everson Dal Piva, Dr. (UFSM)

Vagner Anabor, Dr. (UFSM)

Santa Maria, RS
2022

Declaration

I, Bibiana Culau Lopes declare that the thesis which I hereby submit for the degree Doctor in Meteorology at the Federal University of Santa Maria and Docteur és Sciences (Physique de l'atmosphere), Université de La Réunion is my own work and has not previously been submitted by me for a degree at these or any other tertiary institution.

Signature

Bibiana Culau Lopes

Date: 13 June 2022

This study was financied in part by the Coordenação de Aperfeiçoamento de Pessoal de Nível Superior - Brasil (CAPES) – Finance Code 001

Lopes, Bibiana
Analysis of the UVB radiation during the events of influence of the Antarctic ozone hole over south of Brazil / Bibiana Lopes.- 2022.
81 p.; 30 cm

Orientadora: Damaris Kirsch Pinheiro
Coorientador: Hassan Bencherif
Tese (doutorado) - Universidade Federal de Santa Maria, Centro de Ciências Naturais e Exatas, Programa de Pós-Graduação em Meteorologia, RS, 2022

1. UV Radiation 2. UV Index 3. Antarctic Ozone Hole 4. Brewer spectrophotometer I. Kirsch Pinheiro, Damaris II. Bencherif, Hassan III. Título.

Sistema de geração automática de ficha catalográfica da UFSM. Dados fornecidos pelo autor(a). Sob supervisão da Direção da Divisão de Processos Técnicos da Biblioteca Central. Bibliotecária responsável Paula Schoenfeldt Patta CRB 10/1728.

Declaro, BIBIANA LOPES, para os devidos fins e sob as penas da lei, que a pesquisa constante neste trabalho de conclusão de curso (Tese) foi por mim elaborada e que as informações necessárias objeto de consulta em literatura e outras fontes estão devidamente referenciadas. Declaro, ainda, que este trabalho ou parte dele não foi apresentado anteriormente para obtenção de qualquer outro grau acadêmico, estando ciente de que a inveracidade da presente declaração poderá resultar na anulação da titulação pela Universidade, entre outras consequências legais.

If you want to find the secrets of the universe, think in terms of energy, frequency and vibration."

Nikola Tesla

RESUMO

ANALISE DA RADIAÇÃO UV-B DURANTE OS EVENTOS DE INFLUÊNCIA DO BURACO DE OZÔNIO ANTÁRTICO NA REGIÃO SUL DO BRASIL

AUTORA: Bibiana Culau Lopes
ORIENTADORA: Damaris Kirsch Pinheiro
COORIENTADOR: Hassan Bencherif

A exposição ao sol é fundamental para a saúde humana e para o crescimento e desenvolvimento da flora e fauna, embora a exposição excessiva aos raios UV do sol possa ser prejudicial a todos os seres vivos. Pode afetar animais aquáticos, terrestres, plantas e pode causar sérios problemas de saúde humana, tais como queimaduras, lesões oculares, a exposição prolongada pode levar ao câncer de pele e acelerar o envelhecimento da pele. O ozônio é o principal gás na atmosfera terrestre que absorve a radiação UV na estratosfera. O Buraco de Ozônio Antártico (BOA) caracteriza-se por uma redução extrema dos níveis de ozônio na região antártica na primavera. Os efeitos secundários da AOH são causados pelo deslocamento de massas de ar pobres em ozônio do vórtice polar para as latitudes médias, incluindo o sul do Brasil. Nesta base, este estudo teve como objetivo investigar o comportamento da radiação UV solar, através da análise do índice UV coletado no sul do Brasil (29,4° S, 53,8° O) utilizando dados da radiação UV terrestre (espectrofotômetro Brewer modelo MKIII#167) e de satélite. As medidas na superfície incluem índice UV, dose eritematosa, UV-B não-oesado e integral diária de UV. Os dados de UV usados são do período de 2005-2017, foram comparados com medidas do Instrumento de Monitoramento do Ozônio (OMI) a bordo do satélite Aura. De modo geral, a radiação UV no sul do Brasil, em Santa Maria, é dominada pelo ciclo sazonal anual, com um máximo no verão e um mínimo no inverno. Entretanto, índices UV muito altos e até mesmo extremos foram medidos na primavera e no outono. A análise espectral usando o método wavelet mostrou que a variabilidade UV no sul do Brasil também é modulada por 3 forçantes: a El-Nino Southern Oscillation (ENSO), a Oscilação Quasi-Bienal (QBO) e o ciclo solar. Quanto à influência das anomalias devidas ao efeito secundário do BOA, obtivemos uma redução média de 1% da coluna de ozônio total, com um aumento médio de 4% do índice UV, nas condições de céu claro.

Palavras-chave: Radiação UV. Índice UV. Buraco de Ozônio na Antártida. Espectrofotômetro Brewer.

ABSTRACT

ANALYSIS OF THE UVB RADIATION DURING THE EVENTS OF INFLUENCE OF THE ANTARCTIC OZONE HOLE OVER SOUTH OF BRAZIL

AUTHOR: Bibiana Culau Lopes
ADVISOR: Damaris Kirsch Pinheiro
CO-ADVISOR: Hassan Bencherif

Exposure to the sun is fundamental for human health and the growth and development of flora and fauna, although excessive exposure to the sun's UV rays can be harmful to all living things. It can affect aquatic and terrestrial animals, plants and can cause serious problems on human health, such as burns, eye damage and long-term exposure can lead to skin cancer and accelerate skin aging. Ozone is the main gas in the Earth's atmosphere that absorbs UV radiation in the stratosphere. The Antarctic Ozone Hole (AOH) is characterized by an extreme reduction in ozone levels in the Antarctic region in the spring. The secondary effects of the AOH are caused by the displacement of ozone-poor air masses from the polar vortex to the mid-latitudes, including southern Brazil. On this basis, this study aimed to investigate the behavior of solar UV radiation, through the analysis of the UV index collected in southern Brazil (29,4° S, 53,8° O) using ground (Brewer spectrophotometer) and satellite UV radiation data. The ground-based measurements include UV index, erythemal dose, unweighted UV-B, and daily UV integral. The UV data used covers the period 2005-2017 were compared with observations from the Ozone Monitoring Instrument (OMI) experiment onboard the Aura satellite. Overall, UV radiation in southern Brazil, in Santa Maria, is dominated by the annual seasonal cycle, with a maximum in summer and a minimum in winter. However, very high and even extreme UV indices were measured in spring and fall. Spectral analysis by the wavelet method showed that the variability of UV radiation in southern Brazil is also modulated by 3 forcing: El-Nino Southern Oscillation (ENSO), the Quasi-Biennial Oscillation (QBO) and the solar cycle. As for the influence of anomalies due to the secondary effect of the AOH, we obtained an average reduction of 1% of the total ozone column, with an average increase of 4% of the UV index, under clear-sky condition.

Keywords: UV Radiation. UV Index. Antarctic Ozone Hole. Brewer spectrophotometer.

RÉSUMÉ

ANALYSE DU RAYONNEMENT UVB PENDANT LES ÉVÉNEMENTS DE INFLUENCE DU TROU D'OZONE ANTARCTIQUE SUR LE SUD DU BRÉSIL

AUTEUR: Bibiana Culau Lopes
CONSEILLER: Damaris Kirsch Pinheiro
CO-CONSEILLER: Hassan Bencherif

L'exposition au soleil est fondamentale pour la santé humaine, la croissance et le développement de la faune et de la flore, bien que l'exposition excessive aux rayons UV solaires puisse être nocive pour tous les êtres vivants. Elle peut affecter les animaux aquatiques et terrestres, les plantes et peut causer de graves problèmes sur la santé humaine, tels que les brûlures, les lésions oculaires et l'exposition à long terme peut conduire au cancer de la peau et accélère le vieillissement de la peau. L'ozone est le principal gaz de latmosphère terrestre qui absorbe le rayonnement UV dans la stratosphère. Le trou d'ozone antarctique (AOH Antarctic Ozone Hole) se caractérise par une réduction extrême de la teneur en ozone dans la région antarctique au printemps. Les effets secondaires de l'AOH sont causés par le déplacement des masses d'air pauvres en ozone, du vortex polaire vers les latitudes moyennes, y compris le sud du Brésil. Sur cette base, cette étude visait à étudier le comportement du rayonnement UV solaire, par l'analyse de l'indice UV collecté dans le sud du Brésil (29,4řS, 53,8řO) en utilisant des données de rayonnement UV au sol (spectrophotomètre Brewer) et par satellite. Les mesures au sol comprennent l'indice UV, la dose érythémale, les UV-B non-pondérés et l'intégrale quotidienne des UV. Les données UV utilisées couvrant la période 2005-2017 ont été confrontées aux observations de lexpérience OMI (Ozone Monitoring Instrument) embarquée sur le satellite Aura. Globalement, le rayonnement UV au sud du Brésil, à Santa Maria, est dominé par le cycle saisonnier annuel, avec un maximum en été et un minimum en hiver. Cependant, des indices UV très élevés et même extrêmes ont été mesurés au printemps et en automne. L'analyse spectrale par la méthode des ondelettes a montré que la variabilité du rayonnement UV au sud du Brésil est également modulée par 3 forçages : l'oscillation australe El-Nino (ENSO), l'oscillation quasi-biennale (QBO) et le cycle solaire. Quant à linfluence des anomalies dues à leffet secondaire de lAOH, nous avons obtenu une réduction moyenne de 1% de la colonne totale d'ozone, avec une augmentation moyenne de 4% de l'indice UV, dans les conditions de ciel claire.

Mots clés: UV Radiation. UV Index. Antarctic Ozone Hole. Brewer spectrophotometer.

LIST OF FIGURES

CONTENTS

1 INTRODUCTION

Solar radiation is an essential element of energy budget of the planet, along with its attenuating factors they form an ideal balance allowing life on Earth. All living beings, fauna and flora depend on solar radiation to develop and grow. Solar radiation acts as a source of vitamin D for human beings, which is an important nutrient for metabolism and immune system (ROZEMA et al., 1997; HOLICK, 2008; ENGELSEN, 2010). However, the excess of exposure can be harmful for plants, animals and humans.

Ultraviolet radiation (UV-R) located in the region of electromagnetic spectrum, between 100 nm and 400 nm, is divided in three different wavebands due to its biological effects on humans, plants and animals. UVC- (from 100 to 280 nm), absorbed completely by the atmosphere, so that it does not reach the surface. UV-B, from 280 to 320 nm, is highly absorbed by the atmosphere, especially on the ozone layer, reaching partially the surface and UV-A, from 320 to 400 nm reaches the surface with more intensity because of its absorption on the atmosphere is weak (WHO, 1994).

UV-B corresponds to a high frequency (short wavelength), its intensity is capable of penetrating in deep layer of the skin, causing DNA damage, leading to DNA mutations and development of skin cancer. The most immediate effect is the erythema, the redness on the skin which can lead to sunburn (PFEIFER; BESARATINIA, 2012). There are also several issues related to eye damage because of long-term solar radiation exposure (WANG et al., 2012).

Based on the health matter related to solar radiation exposure, in 1994 it was adopted by the World Health Organization and the World Meteorological Organization the UV Index, a measure of the amount of incident UV radiation on the surface considering the biological sensitivity to UV-R in the UV-B range. The classification is non-dimensional and with a scale of colors, it is intended to be of easy comprehension, it starts in 2 (low), from 3 to 5 (moderate), from 6 to 7 (high), from 8 to 10 (very high) and above 11 is considered extreme (WANG et al., 2014; FIOLETOV; KERR; FERGUSSON, 2010).

Many factors on the planet can cause variability and may influence UV radiation, changing the level of UV index. Attenuation factors include reflection by clouds or the surface, absorption or scattering by clouds or molecules in the atmosphere. Absorption of UV radiation by ozone is one of the most significant mean of attenuation, especially UV-B. It occurs on the ozone layer (10-50 km), which is considered a shield for UV radiation (FIOLETOV; KERR; FERGUSSON, 2010).

The Antarctic ozone hole (AOH), a seasonal phenomenon in this region that occurs during spring of south hemisphere, consists in the extreme depletion of ozone content. During this period air masses poor in ozone travel from Antarctic reaching mid-latitude regions, such as south of Brazil, allowing higher intensity of UV-B radiation to reach the

surface, which is known as the secondary effects of AOH.

Considering the harmful effects of excess exposure to UV-R and evidences reported by many authors regarding the secondary effects of Antarctic ozone hole in the south region of Brazil, the present study aimed to know the behavior of UV radiation during those events of secondary effects of AOH. The study location was in the Southern Space Observatory (29.4° S, 53.8° W), in the central region of the state of Rio Grande do Sul, south of Brazil. Surface UV was collected with a Brewer Spectrophotometer (MKIII #167) (KIPP ZONEN Inc.) between the years 2005 and 2017 (SCI-TEC, 1999).

First, UV index from ground and satellite (OMI/AURA) were compared and seasonal and interannual variations of UV index and erythema were thoroughly studied considering days with all-sky conditions and separately considering only days with clear-sky conditions. Using the wavelet method of analysis, it was observed interannual variations and the possible influence of Quasi-biennial oscillation (QBO), ENSO (El Niño southern oscillation) which influence the surface UV due to their interference on ozone distribution in stratosphere, and also the influence of solar cycle. Finally, the surface UV-R was observed, along with ozone total column, during events of secondary effects of AOH.

1.1 OBJECTIVES

The main goal of the present study is to analyze the behavior of Ultraviolet radiation incident on the surface during events of secondary effects of Antarctic ozone hole on southern region of Brazil, through ground-based measurements collected with a Brewer spectrophotometer between 2005 and 2017, installed in São Martinho da Serra, in the Southern Space Observatory (29.4° S, 53.8° W), and also through satellite measurements.

1.1.1 Specific objectives

Specific objectives addressed in order to develop the present study were:

- Obtain the climatology of the UV radiation incident;
- Determine the seasonal and interannual variabilities of the UV radiation;
- Verify the variation of UV during events of secondary effects of Antarctic ozone hole;

2 THEORETICAL REVIEW

2.1 ULTRAVIOLET RADIATION

A very complex system of fluid temperature and pressure exchanges, molecules and chemical reactions acts on the atmosphere affecting the surface of Earth. Plus, geometrical and motion aspects also influence the climate on surface (STULL; AHRENS et al., 2000). Solar radiation that enters the atmosphere and reaches the Earth's surface plays a key role in the Earth's climate. Not all the radiation emitted by the sun reaches the surface, because between the sun and the surface there are many factors that act to attenuate this radiation. Some of the radiation is absorbed and some is reflected, both by the atmosphere and by the Earth's surface. This results in an equation that includes how much is emitted and how much is absorbed and reflected, called the energy balance (SEINFELD; PANDIS, 2006).

Energy emitted by the sun is an electromagnetic wave that propagates in the atmosphere, it is composed by two components, an electrical and a magnetic that oscillate perpendicular to the direction of spread (BUNGE; BECKERS; GRIES, 2016). Downward radiation from the atmosphere to the Earth is shortwave, while the radiation emitted by the earth is longwave. The wavelength is inversely proportional to its frequency and is related to its energy, thus the shorter the wavelength, the higher the frequency and more intense is the energy. Radiant energy has been organized according to its wavelength in a radiation spectrum (Figure 2.1). The radiation that penetrates the atmosphere are in the infrared, visible and ultraviolet region (OKE, 2002).

Ultraviolet radiation (UV-R), seen in the electromagnetic spectrum in the region between 100 nm and 400 nm, corresponds to approximately 8% of the total radiation emitted by photosphere and chromosphere incident on the top of the Earths atmosphere (ROBINSON, 1966; WOODS et al., 1996). The amount of ultraviolet radiation that reaches the surface is much less, though and it depends on the wavelength since part of it is absorbed in the atmosphere. UV radiation was divided in four: extreme ultraviolet, known as EUV (between 10 and 100 nm), far ultraviolet (from 100 to 200 nm), mid ultraviolet (from 200 to 300 nm) and near ultraviolet (from 300 to 400 nm), according to its wavelengths (COULSON, 1976).

Regarding to the biological effects of UV radiation, it was divided in three: UV-C, UV-B and UV-A. Located in the region of electromagnetic spectrum between 100 nm and 280 nm, UV-C does not reach the surface due to the strong attenuation in the atmosphere by ozone layer, molecular oxygen and other compounds. UV-B in the spectral region from 280 to 320 nm, although it is highly absorbed in the atmosphere, it is one of the most relevant wavebands due to its biological effects, which are being detailed discussed in the

next section (ICSU, 1999). UV-A is in the region between 320 and 400 nm according to KIRCHHOFF (1995). However, ICSU (1999) has defined it starts in 315 nm, it is poorly absorbed by atmospheric gases and mostly of it reaches the surface (WHO, 1994).

Figure 2.1 – Electromagnetic spectrum.

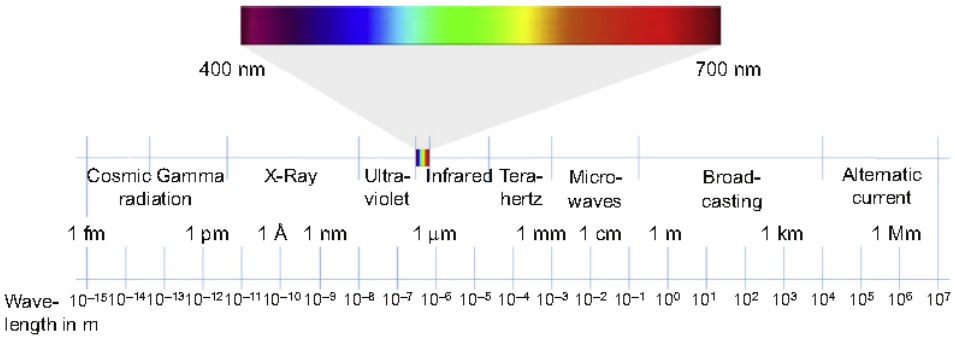

Source: (BUNGE; BECKERS; GRIES, 2016)

2.1.1 Effects of radiation UV-B on ecosystems

Ecosystems can be affected by UV radiation in many ways. Although it is crucial for growth and development of plants and life of fauna depending of intensity of UV-B radiation, it can cause DNA lesions and mutations in plants and animals, among other damaging effects including in aquatic systems (ROZEMA et al., 1997; CADET; SAGE; DOUKI, 2005; GARCÍA-HUIDOBRO et al., 2017).

In addition, depending on the level of UV-B radiation it can provide a stressful environment for terrestrial plants, including crops because its locomotion impossibilities, lack of adaptation and tolerance to UV summed with its ability to absorb UV-R can lead to great photobiological effects, such as damage in biological macromolecules as proteins, lipids and nucleic acids. Moreover, a very strong indicator of harmful potential of UV-B radiation is DNA damage because it is the main cause of cell degradation (TERAMURA, 1983; KAKANI et al., 2003; JANSEN; NOORT, 2000; MALLOY et al., 1997).

Different profiles of lesions on DNA were identified with solar exposure which also vary with location, besides different solar zenith angle cause more or less intensity in UV-B, the genotoxic potential of sunlight changes with different latitudes. Solar UV radiation is able to damage biomolecules which changes DNA structure and might lead to mutations affecting cell functions (SCHUCH et al., 2012).

Besides DNA damage, it was observed that increase in UV-B in the early spring in south American region, period coincident with events of Antarctic ozone hole, which will be further discussed in following sections, can affect leaf growth of native plants (ROUSSEAUX

et al., 1999).

Water bodies communities can be affected by the increase of temperature due to increase in UV-B intensity and by the incidence of UV radiation itself. Among the consequences is the increase in oxygen consumption associated with a major energy waste in order to repair damage caused by UV radiation in fish (GARCÍA-HUIDOBRO et al., 2017). An entire food chain could be undermined by the increase of UV-B radiation in the ocean. Damages can start in phytoplankton even in 20 meters dept in clear waters and also zooplankton organisms can suffer irreversible damage leading to the mortality of species and a decline in fish (DIFFEY, 1991).

Schuch (2009) studied DNA damage induced by UV radiation and its genotoxic effects confirming DNA photoproducts are the most significant factors in the induction of genotoxic effects of UV radiation, artificial and natural sources. Many studies have related those negative effects of UV-B radiation on ecosystems with the ozone changes affecting UV radiation levels (FARMAN; GARDINER; SHANKLIN, 1985). Decline of amphibious species in mid latitude regions affected by Antarctic ozone hole was associated with the consequently increase of UV-B, besides that higher rates of malformation were observed in individuals irradiated with UV-B (SCHUCH et al., 2015).

2.1.2 Effects of radiation UV-B on human health

UV-R exposure is linked to many and great biological effects on human being, probably due to the fact it is a short wave, its high intensity can penetrate deeper layers of skin and even affect DNA (PARKER, 2014). As mentioned, it was divided into three classifications, UV-B though even being essential for life on earth, excessive exposure can cause serious damage to health, such as skin burns, premature aging, and even skin cancer (PFEIFER; BESARATINIA, 2012; WANG et al., 2012).

Healthy effects of solar radiation for human being can be exampled as the synthesis of vitamin D, an essential hormone that acts as an immunity booster, it contributes to skeleton and bone metabolism and the lack of vitamin D in human body can result in osteoporosis. Deficiency of vitamin D is defined by Institute of Medicine as 25(OH)D level of less than 20 ng/mL, and it was also associated with autoimmune disorders, infectious and cardiovascular diseases, childhood dental caries, type 2 diabetes and neurological disorders (HOLICK, 2008; ENGELSEN, 2010; HOLICK, 2017).

The synthesis of vitamin D is on the skin, firstly provitamin D3 is converted in previtamin D3 with solar incidence, then a temperature dependent equilibrium processes form vitamin D3. Further reactions include the degradation of vitamin D, also through UV radiation incidence, into suprasterol I, suprasterol II and 5,6 trans-vitamin D3, the following reaction is the transport from the skin to the blood as a D-binding protein that will play im-

portant role in cellular functions, in keratinocytes and immunocompetent cells (DIJK et al., 2016; LEHMANN; QUERINGS; REICHRATH, 2004).

During the pandemics of Coronavirus, named COVID-19, starting in the end of 2019 (GROSS et al., 2020) aroused the importance of having a strong immune system. Many studies were released since then and proving the importance of vitamin D to improve nutritional defense against the infection. Vitamin D improves the defense against viruses and the production of antimocrobial peptides (BAE; KIM, 2020). A study conducted by Rastogi et al. (2022) tested high dose of vitamin D and placebo in adults between 36 and 51 years old that tested positive for COVID-19 and who had vitamin D deficiency, resulted in more than 60% of individuals recover after 21 days. It is not only relevant in the prevention of infection but vitamin D also is important in the attenuation of most severe consequences of COVID-19 (GRANT et al., 2020; HRIBAR; COBBOLD; CHURCH, 2020; RHODES et al., 2021).

Therefore, harmful effects of UV radiation on human beings are normally due to the excess exposure which might cause short- and/or long-term health problems. An example of short-term effect is the erythema, the redness on the skin provoked after certain time of exposure, it varies with time and skin type (DIJK et al., 2016). Erythema caused in different types of skins will be further explained in following sections.

Long-term exposure to UV-R and the successive sunburns can lead to development of skin cancer. Human skin is a complex and large organ with a very detailed renovation and repair system. New cells are created and brought from basal layers to the surface in order to substitute the skin peeling and in case of physical injure, skin cells activate a mechanism in order to repair. UV-R exposure can cause different lesions on the skin, such as the excessive multiplication of those basal cells forming a salient scar, a carcinoma. Lesions in pigment cells lead to melanoma, also causing the same effect of uncontrolled growth of cells forming a hyperpigmentation (PARKER, 2014).

2.1.3 Erythema dose and UV index

Erythema is the redness of the skin resulted from augment of blood content due to dilatation of superficial blood vessels in dermis skin layer as a response to the excessive sunlight and UV exposure. The erythema action spectrum is defined as the effectiveness of UV, in different wavelengths, in causing sunburn, so that it is the basis of UV index, which is used for public health information. Figure 2.2 is the action spectrum applied for three different biological organisms, it shows the relative effectiveness of different wavelengths and response for plant damage, DNA damage and erythema damage. The region of action spectrum of DNA damage is around 315 nm, in UV-B range and the region corresponding to erythema damage starts around 310, also in UV-B range (DIFFEY, 1991; CALDWELL,

1971; SETLOW, 1974; DIFFEY, 1987).

Figure 2.2 – Action spectrum induction Erythema, DNA and plant damage between 280 nm and 400 nm. All three spectra are normalized to unity at 300 nm.

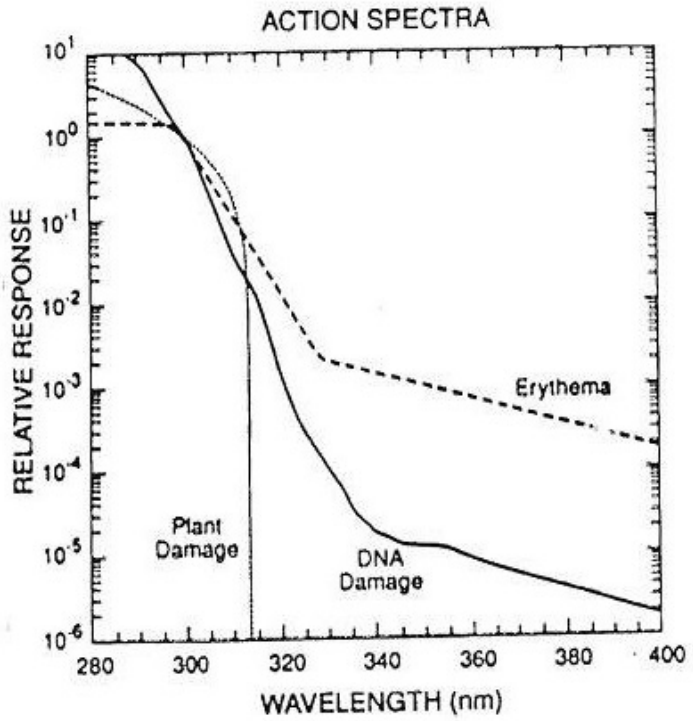

Source: Chapagain, 2019.

Standard erythema dose (SED) is the total erythemal radiation received and it is quantified as 1 SED equals to 100 Jm^{-2} of erythemal effective radiation. The term Minimum Erythema Dose (MED) (Jm^{-2}) refers to the sensibility of each type of skin to UV radiation, considering the skin pigmentation and intensity of exposure (ILLUMINATION, 2019). It does not express one singular value because it varies from person to person, mostly according to the skin type. Thus, a classification of photo types (Figure 2.3) was created based on sensibility of each skin type to sun exposure. A dose from 250 to 300 Jm^{-2}, can cause erythema in photo types I and II, a dose from 450 to 600 Jm^{-2} can affect photo types III and IV (FITZPATRICK, 1988).

Using the SED and action spectra it is possible to calculate the accumulated erythemal dose (DOSE), in a certain period of time, in units of energy per area, with Equation 2.1, where S is the solar irradiance biologically active in Jm^{-2} and at a period of time (ΔT) (minutes) (COARITI, 2017).

$$DOSE = S * \Delta T \quad [Jm^{-2}] \tag{2.1}$$

Figure 2.3 – Skin classification.

SKIN TYPE CLASSIFICATION		BURNS IN THE SUN	TANS AFTER HAVING BEEN IN THE SUN
I. II.	Melano-compromised	Always Usually	Seldom Sometimes
III. IV.	Melano-competent	Sometimes Seldom	Usually Always
V. VI.	Melano-protected	Naturally brown skin Naturally black skin	

Source: World Health Organization, 2002.

UV index is a non-dimensional scale and is related to the human skin response to UV radiation exposure, it informs the population of the amount of radiation they are being exposed to. Equation 2.2 is showing that UV index is calculated considering the skin response to the exposure to UV radiation through the erythema action spectrum ($S_{er\lambda}$), the solar spectral irradiance (W/m^2.nm^{-1}) between wavelength interval used ($d\lambda$), K_{er} is a constant equal to 40W/m^2.nm^{-1}, used to covert UV index into a non-dimensional value as seen in (Figure 2.4) (ORGANIZATION et al., 2002).

$$UV_{index} = K_{er} \int_{280nm}^{400nm} E_{\lambda} S_{er}(\lambda) d\lambda \tag{2.2}$$

Figure 2.4 – UV index range and scale of colors.

EXPOSURE CATEGORY	UVI RANGE
LOW	< 2
MODERATE	3 TO 5
HIGH	6 TO 7
VERY HIGH	8 TO 10
EXTREME	11+

Source: World Health Organization, 2002.

A typical daily behavior of UV radiation considering a scenario of clear sky during all day can be seen in Figure 2.5, it also includes an example of possible UV index distribution along the day. Irradiance intensity increases during the day, starting very low as the sun rises and with the highest peak of UV radiation being around noon time when the sun is at highest in the sky, decreasing along the afternoon, forming a Gaussian curve. Thus, depending on the time of day, there are different levels of UV index and, depending on the UV index, it is required protection measures, as it is indicated in Figure 2.6 (FIOLETOV; KERR; FERGUSSON, 2010; ORGANIZATION et al., 2002).

Figure 2.5 – UV index daily behavior.

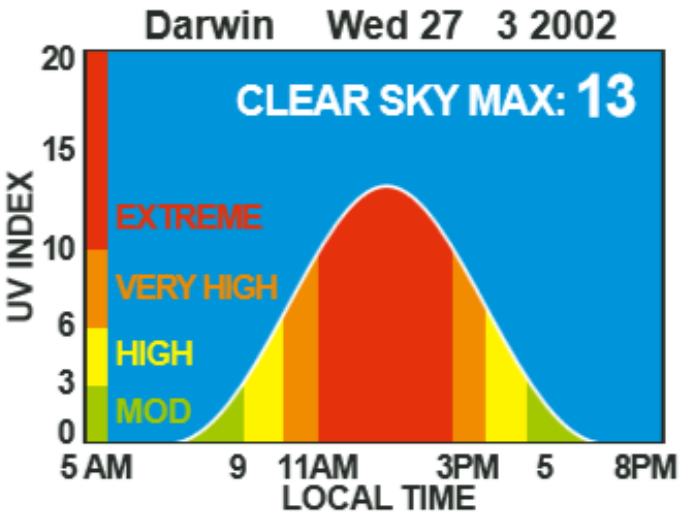

Source: World Health Organization, 2002.

Besides the tendency of less intensity in UV radiation at certain periods of day and different responses to sun exposure depending on the photo type, it is recommended fare attention to sun exposure since erythema doses may exceed the recommended amounts mainly in summer season and offer risks mostly to people with skin type I (CORRÊA; PIRES, 2013).

Figure 2.6 – UV index protection measures.

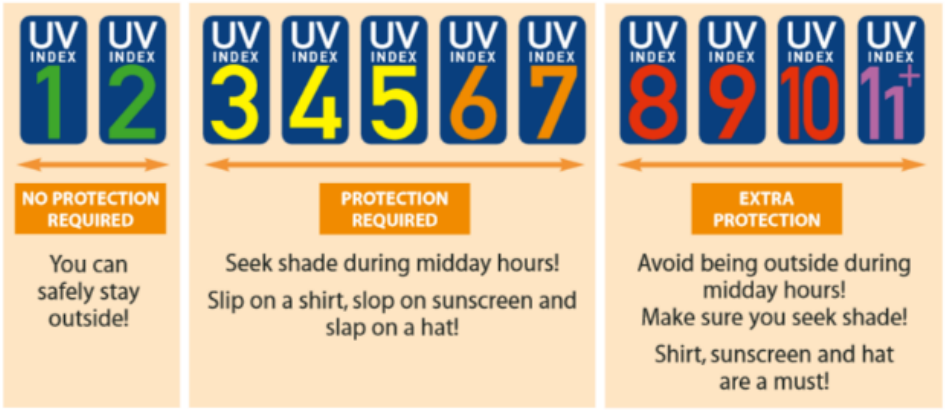

Source: World Health Organization, 2002.

2.1.4 Attenuation of ultraviolet radiation

In different aspects atmosphere and its constituents, as well as Earths surface interact with UV-R influencing in its intensity, either by absorption, scattering or reflection of radiation, as it can be seen in the illustration of Figure 2.7. Geographical aspects, for

instance, include altitude of site. Higher locations account with thinner atmosphere, therefore less attenuating mean so tend to have more incidence of radiation. It is estimated for each kilometer of altitude above sea level, there is an increase of UV between 7% and 15% (SCHMUCKI; PHILIPONA, 2002; ZARATTI et al., 2003). The latitude is also relevant because regions closer from equator are more exposed to UV radiation (COARITI, 2017).

Regarding to Earths surface, the higher the capacity of a surface in reflecting UV-R, the higher the albedo is, so the more radiation is in the area. Generally, water bodies and land have low albedo, even less than 5%, on the other hand, sand surfaces have higher albedo. Ice and snow have much higher, specially a smooth terrain, with fresh snow can reflect 85% to 90% of UV radiation (WEBB et al., 2004; PARISI et al., 2003; DIFFEY, 1991).

Figure 2.7 – Illustration of Earths energy budget showing the path of incoming solar energy passing through attenuation mean until it reached the surface, as well as the estimated energy reflected and absorbed.

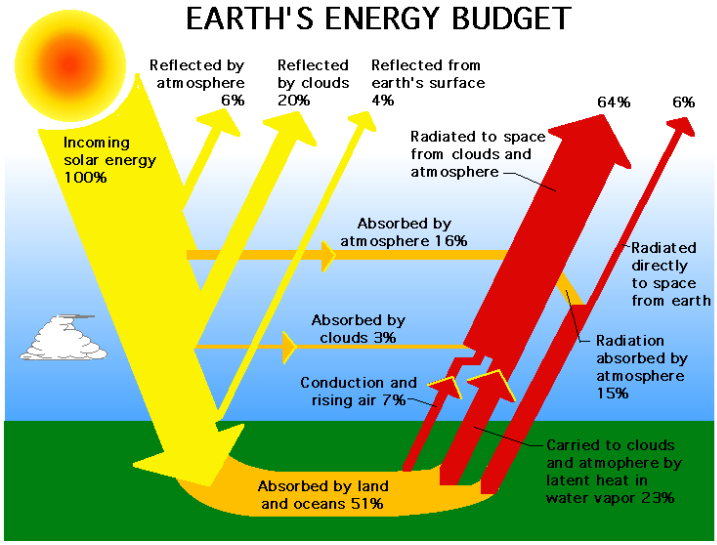

Source: NASA GPM, 2022.

Astronomical aspects include solar declination and it is related with solar zenith angle. Considering a location of an observer on Earths surface, the angle between the sun and the perpendicular line (zenith) at observers location. The most proximate to zero or the more overhead the sun is, the angle indicates the solar flux is more intense at the site, since the irradiance of solar radiation is proportional to the cosine of solar zenith angle. Furthermore, with the increase of solar zenith angle direct irradiance coming from the sun has a longer path to pass through atmosphere and reach the surface, besides that, suffering more attenuation of the mean (SEINFELD; PANDIS, 2006; FIOLETOV; KERR; FERGUSSON, 2010).

Distance between Sun and Earth, the tilt of the Earths axis relative to a line perpendicular to the ecliptic and solar declination angle (δ), defined as the angle between the ecliptic and the plane of the Earths equator. Those features are directly linked to seasonal

variations in both hemispheres, which leads to temporal aspects, as time of day and time of year. Solar declination angle smoothly varies along the year, δ=+23°27' N and δ=-23°27' S. When solar declination is lowest (δ=-23°27' S) it is summer solstice in Southern hemisphere, UV radiation is more intense (STULL; AHRENS et al., 2000).

Atmospheric processes encompass the interaction of UV radiation with gases, aerosols and clouds that can result in photo reactions. Three different interactions mechanisms can be cited. Absorption, molecules of gases absorb the energy of UV radiation releasing heat in the process. Depending on the amount of energy, it might result in a separation of atoms of the molecule that is absorbing the energy, and then there is heat emission due to this breakdown. Reflection, the radiation reaches a surface and the energy changes direction being reflected in the direction of the beam.

And scattering, radiation hits a molecule and it re-radiates this energy. Depending on the symmetry of the molecules, different types of scattering can occur. When there is forward energy scattering it is called Mie scattering, when there is both forward and backward energy scattering of the molecule then Rayleigh scattering occurs (LIOU, 2002).

Aerosols can either reflect and scatter solar radiation, they consist in particles suspended in the atmosphere that vary in size, between 0,01 and 100 μm of diameter, solid or liquid they interact with climate, participate in radiative processes and also influence in public health. Natural sources of aerosols are sand from beaches and desert, salt from the ocean, dust carried with wind, volcanos and forest fires. Anthropogenic sources of aerosol are industrial activities, emissions from fossil fuels, power plants, factories, thus load of aerosols in urban areas tend to be higher (ARTAXO et al., 2006; ORGANIZATION; CONTROL, 2008; SEINFELD; PANDIS, 2006; FIOLETOV; KERR; FERGUSSON, 2010; SARRA et al., 2002).

UV radiation is mostly scattered by aerosols, specially aerosols from anthropogenic sources. It is estimated that 5 to 18% of UV-B reaching the surface has decreased since the industrial revolution in industrial areas (LIU; MCKEEN; MADRONICH, 1991). Changes in UV radiation due to aerosol variations were compared to the changes in UV radiation due to ozone changes, estimating that 10% increase in aerosol optical depth would result in approximately 1,5% decrease in UV erythemal daily dose (KRZYŚCIN; PUCHALSKI, 1998).

Clouds attenuate UV radiation either by reflecting, scattering or absorbing it depending on the cloud type. The most significant reduction is in visible light region while in ultraviolet is not so great in terms of intensity reduction, which draws the attention to the risk of exposure even in cloudy days. Although a complete cloud cover sky scenario can reduce UV radiation in half when compared with clear sky, heavy storm clouds can reduce even more during summer (STULL; AHRENS et al., 2000; DIFFEY, 1991; CORRÊA, 2015).

Generally, thicker clouds located at lower altitudes tend to reflect solar radiation, in contrast, higher and thinner clouds transmit solar radiation. Altitude, thickness, size and

formation of cloud droplet are important factors related to cloud interaction with radiation. Clouds have high albedo and normally reflect energy back to space, contributing with cooling of the surface. Clouds with colder tops tend to trap the energy instead of reflect and in this way contribute with higher temperature on Earths surface. Cloud reflectivity can also be significant in reflecting UV radiation downward to the surface which may cause enhancement of UV radiation intensity in the surface (SMITH; OWENS, 2003; TIBA; LEAL, 2017).

Regarding to interactions between molecules in the atmospheric mean and UV radiation, there are many photo reactions occurring. Some molecules are highly reactive and solar energy acts dissociating those compounds into fragments, it depends on the energy of the photon concerning the molecule. The level of absorption of solar irradiance by molecules varies in the atmosphere. In some regions, absorption is extremely strong at a point there is no incoming energy, for example oxygen and ozone strongly absorb incident radiation at UV-C wavelengths. Whereas in other region of the spectrum, 300 to 800 nm the absorption is quite low, forming the so-called window in the spectrum. UV radiation is also absorbed but mainly by ozone in the Hartley band (SEINFELD; PANDIS, 2006).

2.2 OZONE LAYER, ANTARCTIC OZONE HOLE AND ITS SECONDARY EFFECTS

The most important absorption of UV radiation by molecules is by ozone (O_3), it is the only atmospheric gas that absorbs at wavelengths below 320 nm, thus it acts as a filter for all species and to the surface. Ozone greatest concentration in the atmosphere is located in the stratosphere, between 10-50 km above the surface, where about 90% of its concentration is found. A column is measured with Dobson Units, for instance, 1 mm thick layer of a vertical column corresponds to 100 Dobson Units (DU) (ORGANIZATION; CONTROL, 2008).

A process of photolytic decomposition naturally happens producing and destroying ozone in the stratosphere, UV radiation is absorbed, mainly UV-C by oxygen (O_2) leading to its dissociation, in this process heat is released resulting in the warmth of the stratosphere layer. The molecules later associate again forming O_2 and O_3. The ongoing process of destruction and formation of Ozone is called Chapman cycle. Thus, the major formation of O_3 occurs where the sunlight is more intense, in the tropical stratosphere, however, the greatest amount of O_3 concentration ends up to be in middle and high latitudes (SEINFELD; PANDIS, 2006).

The meridional transport of ozone from the tropics to the poles, in the lower stratosphere happens through the Brewer-Dobson circulation, showed in Figure 2.8 (BREWER, 1949; DOBSON, 1956). It consists in a vertical ascendance of air masses on the tropics, that are distributed in poleward of both hemispheres carrying ozone to the pole regions,

being more effective in winter hemisphere. The air masses reaching the pole regions in the upper stratosphere mix with the mean and descend on the polar vortex (PLUMB, 2002). The stratospheric air returns to the tropics through its descendance to the troposphere in higher latitudes (FLURY; WU; READ, 2013).

Figure 2.8 – Diagram of the Brewer-Dobson Circulation.

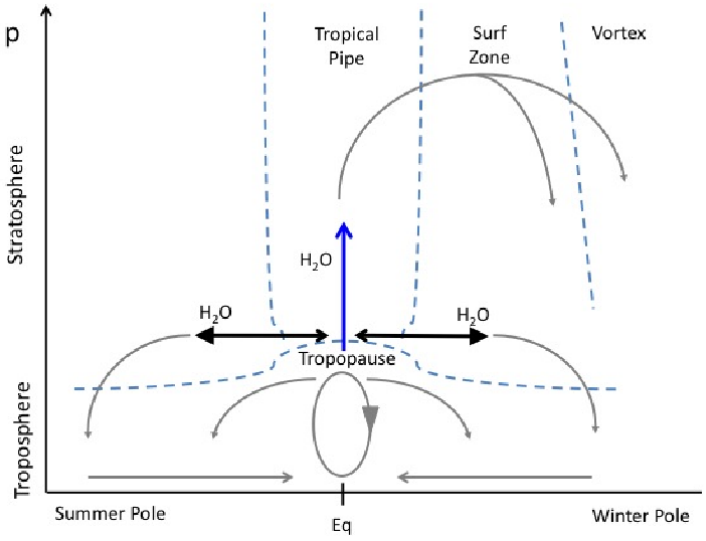

Source: FLURY; WU; READ, 2013.

Brewer-Dobson circulation defines ozone transport between stratosphere and troposphere in global and hemispherical scale but also carries other atmospheric gases with it, modulating temperatures in tropopause, water vapor in stratosphere and other important process regarding to the climate of Earth (FU et al., 2019). It was found in early 1970s manmade compounds, such as chlorine, fluorine and carbon atoms, would contribute for ozone destruction (MOLINA; ROWLAND, 1974).

A significant drop in ozone total column in the lower stratosphere in Antarctic region was detected and it was firstly reported in 1985 by Farman, Gardiner & Shanklin (1985). It was the ozone hole, that continues to occur, annually, during the austral spring on the Antarctic region. Characterized by ozone levels decreasing down to 220 DU, its cause was attributed to the destruction of ozone molecules by chlorofluorocarbons compounds (DOUGLASS; NEWMAN; SOLOMON, 2014; HOFMANN et al., 1997).

The features of seasonality and location of Antarctic ozone hole are due to a series of processes that start in the beginning of winter in South hemisphere. Antarctic region goes dark and polar temperatures falls, a strong jet stream from west speeds up due to pressure gradient and Coriolis effect, forming the polar vortex that reaches altitudes between 50 to 80 km. Gases as CFCs are carried withing the Brewer-Dobson circulation and descend in the core of the vortex. In spring with solar radiation reaching the vortex photocatalytic reaction with those compounds create radicals that will later react and destroy ozone (DOUGLASS;

NEWMAN; SOLOMON, 2014).

During spring the polar vortex weakens gradually, becoming less stable and ozone-depleted air masses get released and move to low latitudes, in populated areas, carrying the low ozone content with it for those regions. The last described process characterizes the secondary effect of the Antarctic ozone hole (MARCHAND et al., 2005). As it has been reported by Kirchhoff et al. (1996), a significant decrease in ozone on the region of Santa Maria RS, south of Brazil, location where this study was held.

Events of secondary effects of Antarctic ozone hole have been studied in last few years by authors in South America. A large number of those events were identified showing the motion of ozone-poor air masses reaching south of Brazil, lowing ozone total column of the region and still, they can be persistent for a couple of days in the region (BITTENCOURT et al., 2018b, 2018b; PERES et al., 2013; PERES et al., 2016).

In a scenario where there is a reduction of ozone total column, there is a tendency of increase in UV radiation since stratospheric ozone main role is to filter UV radiation by its absorption and thus protecting fauna, flora and humans from the noxiousness of excess exposure to UV radiation (SEINFELD; PANDIS, 2006; CASICCIA; ZAMORANO; HERNANDEZ, 2008).

Ozone depletion during spring time, the period of Antarctic ozone hole, triggers a sequence of many impacts on the terrestrial ecosystem, also affecting climate and public health. In the southern area of Argentina, in South America, close to the Antarctic vortex region it was found that the Antarctic ozone hole led to the increase of surface UV-B resulting in DNA damage of native plants, besides that, in this region the ozone total column depletes down to 50% when compared to the previous years. After 1982 the region of Antarctic ozone hole vortex started to reach the region of Ushuaia causing the great depletion in total ozone column (ROUSSEAUX et al., 1999).

There are prospective studies showing the tendency in increase of ozone total column on the 21^{st} century, which could provide more protection to solar UV exposure. On the other hand, there is the concern with lack of exposure regarding to vitamin D synthesis and its implications on human health. However, Correa et al. (2019) showed that the increase in ozone total column would not result in a tendency reduction of erythema dose in mid-latitude regions, on summer season. So that the increase in ozone total column would not be of enough significance to cause protective effects from UV radiation.

2.3 OSCILLATIONS WITH INFLUENCE ON UV RADIATION

2.3.1 Quasi biennial oscillation and 11-year solar cycle

Other oscillation that causes changes in surface UV radiation is the Quasi Biennial Oscillation (QBO). It consists in alternation of zonal winds, westerly and easterly in the equatorial stratosphere (TROSHICHEV; GABIS, 1998). The oscillation of the wind happens every 2 years, approximately, and the change have origin in the Hadley cell, region of ascendance, in the intertropical convergence zone where there is energy accumulated due to phase change. Hot-air masses rise, mix with colder air masses above forming precipitation clouds, leading to an energy discharge.

The energy burst provokes wave propagation in horizontal and vertical directions. Waves in the vertical directions reach stratosphere layer encountering resistance in vertical transport, those waves break horizontally and propagate in descendent direction from east and west. The intensity of the descendent motion process is dictated by the amount of energy released from precipitation clouds in the intertropical convergence zone (LINDZEN; HOLTON, 1968).

Influence of QBO in UV radiation is also connected with changes in ozone distribution caused by QBO, being this oscillation considered the major persistent sources of ozone variability (BOWMAN, 1989). Herman et al. (2000) found that the most important effects on UV exposure caused by QBO happens in the equatorial regions. And the variabilities in ozone, consequently in UV-B exposure, caused by QBO are greater than decadal trends as well as interannual variabilities such as those caused by clouds.

Quasi biennial oscillation is also associated with changes in the Brewer-Dobson circulation. Interannual variation of Brewer-Dobson circulation speed depends on the QBO phase. An anomaly in meridional circulation caused by QBO impacts the transport to mid-latitudes and vertical ascension in tropical stratosphere. In QBO easterly phase shows maximum ascent rates, while in QBO westerly phase the opposite happens (FLURY; WU; READ, 2013).

There is another concern regarding influence of QBO in UV irradiance that is the relation between QBO and 11-year solar cycle. It is related to sun activity modulated by the flip in its magnetic field every 11 years. The cycles affect sunspots, on solar minimum, for instance there are the least solar spots and solar maxima presents the most sunspots besides solar flares and coronal mass ejections (HATHAWAY, 2015).

In short-term variabilities solar cycle is linked to QBO. There is an atmospheric response to 11-year solar cycle, which affects stratospheric polar temperature. Solar minima, polar-night vortex is warmer during QBO easterlies phase than QBO westerlies phase (SALBY; CALLAGHAN, 2000).

Elias & Artigas (2003) made an interesting relation between solar activity, QBO phase and UV irradiance. Founding that there is periodicity in UV irradiance associated with QBO in atmosphere. And in periods of solar maxima the higher levels of UV are in QBO easterly while the lower levels of UV are associated with QBO westerly phase in solar minima.

2.3.2 El Niño southern oscillation

El Niño-Southern Oscillation (ENSO) is also related with ozone layer alterations impacting in the UV radiation on the surface Manatsa & Mukwada (2017). ENSO is a phenomenon in tropical Pacific resulted by great and sprawling interactions between ocean and atmosphere. It is associated with extreme changes in climate, such as drought, flood, cold and heat wave. ENSO varies in phases, being La Niña consisting in the temperature of sea surface in Pacific cooler than normal while the El Niño happens with the warming of sea surface temperature (METOFFICE, 2022). As ENSO is related with extreme events like drought, it directly impacts temperatures and increase of UV radiation levels, due to long periods without precipitation and less clouds attenuating UV irradiance (JÚNIOR et al., 2020).

The cycles between El Niño and La Niña, shift every two to seven years bringing changes to the climate and also regulating lower stratospheric ozone, mostly in ozone total column in mid-latitude regions, consequently affecting UV radiation in surface (ZHANG et al., 2015). El Niño phase can influence Brewer-Dobson circulation, causing a reduction of ozone transport, leading to less absorption of UV and resulting in a lower temperature in atmospheric layer. The anomalous effect is the reduction in temperature of lower stratosphere, the opposite happens during La Niña phase (MANATSA; MUKWADA, 2017).

3 METHODOLOGY

3.1 STUDY LOCATION

Southern Space Observatory (SSO) is located in São Martinho da Serra, central region of the Rio Grande do Sul state, in the South of Brazil. SSO is one of the research centers of National Institute of Space Research (INPE) in partnership with Federal University of Santa Maria. Gorund instrument used in this study is located on a platform next to building 1, seeing in Figure 3.1

Figure 3.1 – a) Southern Space Observatory (29.4° S, 53.8° W), State of Rio Grande do Sul, Brazil. b) Building 1 and beside the platform where ground instrument is located, (b) Brewer Spectrophotometer MKIII #167

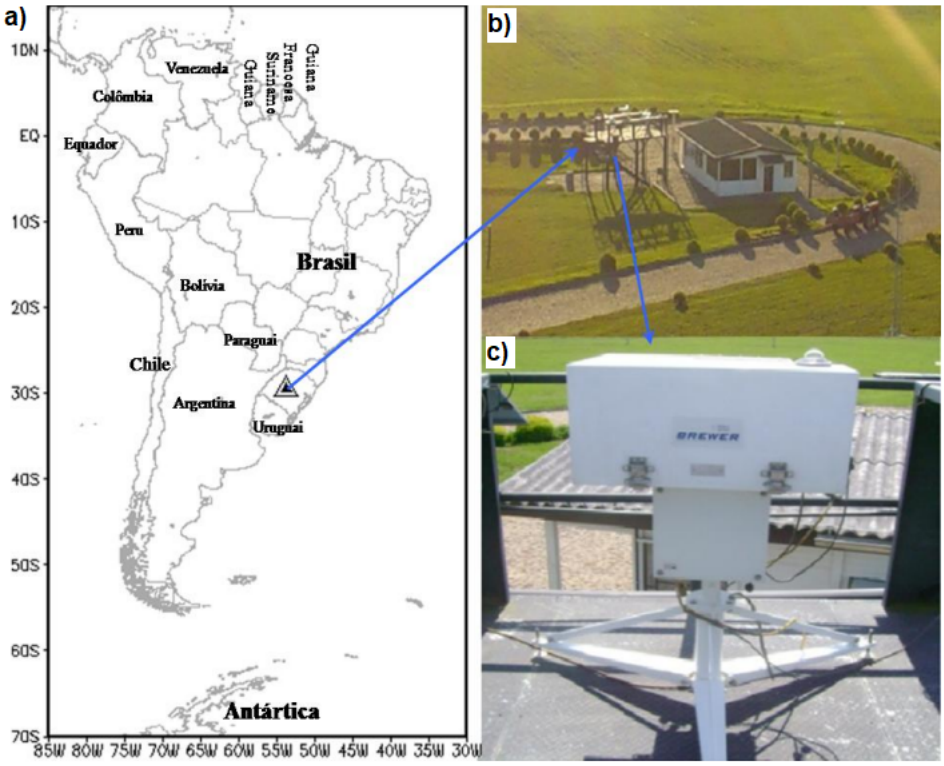

Source: (PERES et al., 2013)

3.2 BREWER SPECTROPHOTOMETER

The equipment measures ultraviolet radiation in the solar spectrum. It is able to determine the Total Column Ozone and Total Column Sulphur Dioxide by examining the

differential absorption of select wavelengths in UV-B portion of the spectrum. The whole Brewer system consists in three main parts, the solar tracking system, a personal computer operating Brewer software and the core component Brewer spectrophotometer (SCI-TEC, 1999).

Brewer runs in either manual or fully automated mode of operation, so it is able to run unattended for long periods, due to a feature of its software, which executes a series of commands, previously set, and is triggered by the Sun when it reaches the Solar Zenith Angle (SZA). The main purpose is to capture light through an entrance slit and disperse it in high-quality spectrum in an exit slit where wavelengths are adjusted and exposed one at a time (SCI-TEC, 1999).

The model MKIII #167, used in this study, contains double optical system (Figure 3.2) offering accuracy in the isolation of wavelengths selected due to its wide radiation spectral and good resolution. The measurements of UV radiation are done every 5 minutes and in a spectral range that goes from 286.5 nm to 363.0 nm with a resolution of 5 nm. The instrument measures ground-level intensities of the attenuated solar ultraviolet radiation, being the attenuating mean the atmospheric column (SCI-TEC, 1999).

Figure 3.2 – Double Optical system of Brewer Spectrophotometer.

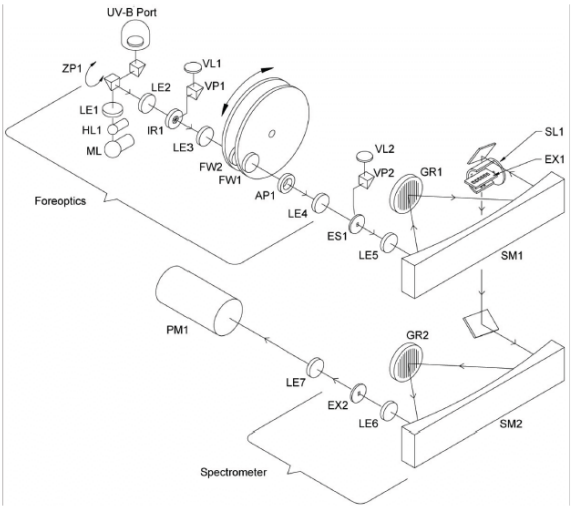

Source: SCI-TEC Instruments Inc., 2019.

Measurements of ultraviolet radiation are done by the entrance of solar radiation through the dome, indicated in Figure 3.2 by UV-B Port, where it is conducted by a prism to a series of lenses, filters, collimators, slit masks, mirrors and the diffraction grid and then reach a cathode in a photomultiplier tube. The light beam is converted in an electric signal and read as a pulse. As it was mentioned, the model MKIII contains two diffraction grids, light beam is reflected by a second spherical mirror, which conducts the light to the second diffraction grid, only then the light beam reaches the photomultiplier (SCI-TEC, 1999).

3.2.1 Brewer spectrophotometer data process

Data files stored by Brewer software regarding to ultraviolet measurements that are relevant and used in this research are the UV files, Lamp files, QL files and UVR response files. UV files contain the UV observations, they are the result of the irradiance over B region of the spectrum. The UV spectrum is scanned in steps of 0.5 nm from 290 nm to 325 nm, the data files generated are named as UVJJJYY.nnn, JJJ corresponds to the Julian date and YY the year, nnn is the number corresponding to the Brewer model. This file contains information of number of cycles, day, month, year location, latitude and longitude of the measurement, among others, there are 15 to 18 lines of information from the scans. The observation of UV-B comes from the irradiance over the B region of the spectrum measured, in a practical way the zenithal prism of the instrument is rotated to the dome, which opens the iris and the tracker reaches suns direction, so that UV spectrum is scanned, all data collected is registered in UV file (SCI-TEC, 1999).

Lamp files are created in the factory by its first and initial scan, the LAMP_LL.nnn contains the Julian date, distance from lamp filament to diffuser, temperature, dark count, intensities at 11 wavelengths, DUV calculation based on the lamp intensities or irradiance. The QL_LLL.nnn is also a Lamp file, which contains more information than the first file, such as the total amount of wavelengths measured and corrected intensities at 24 wavelengths. During the calibration of the instrument it is compared simultaneously standard lamps with lamps inside the instrument. The diffraction grid makes readings of the irradiance of the lamps at each 3.5 nm and at each wavelength, those readings result in the QL file.

UV response files are generated in LampsPro software, for every calibration made in the instrument, one UV response is created with information on the lamps irradiance. Those are essential in data processing because the UV response files are used in the conversion of raw data into irradiance data.

The data processing was done firstly in the software LampsPro to generate the UV response file which was used in the UVBrewer software in order to convert raw data collected during measurements into irradiance and daily integral values. The procedure in LampsPro software consists in selecting the QL, generated in each calibration, and checking which lamp was calibrated in the corresponding year as well as the Julian day of the calibration. Figure 3.3 contains an example of the data collected in the year of 2016. It is possible to observe that in that year, the calibration was done with all the four lamps and as each lamp is selected it is possible to know the Julian day.

The procedure was done by checking the same date for every lamp that has calibration in the corresponding date. After that some configurations must be set in the window. Among the configurations, it is requested to select files with the IRR extension, which are the Lamp response files. As mentioned previously, those correspond to original files from equipments first calibration, it is a factory file used as reference for lamp irradiance.

The software spectrophotometer UV Data Files Analysis Program - UVBrewer was

Figure 3.3 – Software LampsPro.

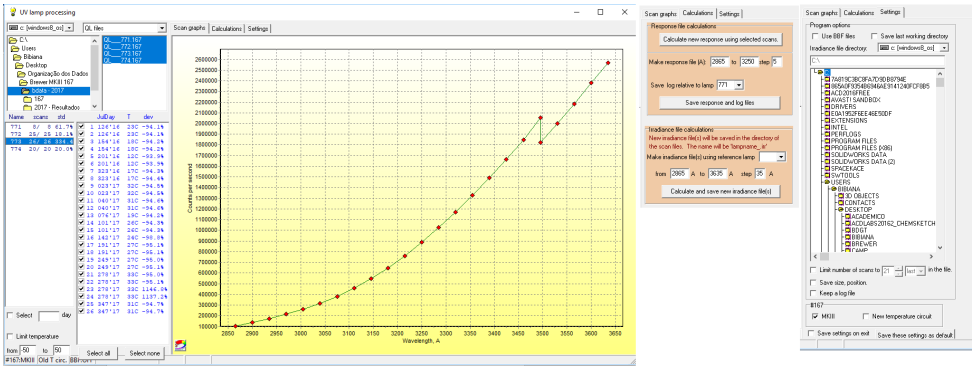

Source: Author.

developed by the engineer Martin Stanek and it is used to analyze ultraviolet radiation generated in the measurements. Raw data are processed in the software that converts the counting into irradiance and daily integral. The program also allows the application of action spectrum, obtaining weighted irradiance according to the spectrum, erythema filter, for example, corresponds to the attenuation regarding to biological spectrum (STANECK, 2008).

UV and UVR files were used in UVBrewer and every day of measurement was analyzed separately, for all years of data processed it was used an average of one UV response file for every 20 days. The information retrieved from processing included the daily irradiance, UV index and erythema. Figure 3.4 contains a graphical example of weighted UV, the distribution of UV in this example represents an open sky day because the data points plotted form a very smooth Gaussian curve, representing the typical behavior of UV radiation along one day. Clouds interfere lowing UV radiation and they are normally detected on the graph through spikes, as it is represented in Figure 3.5, in the region of 4 PM, GMT time. This is also an example of an image extracted from the UVBrewer software.

As it was mentioned above, UV response files (UVR) are created from every calibration of the instrument. The calibration itself is very important because it does an evaluation of the optical and electrical system, indicating the depreciation of the lamps, since the irradiance of the lamps tends to decay with time and so its efficiency affecting the results of UV. So that, the UV response files were analyzed one by one and compared among each other, for all years of the data series.

3.2.2 Brewer data sets

Data processing in Brewers software allowed to extract data regarding to UV index and erythema, also during the processing it was observed the curve corresponding to the solar UV irradiance of each day of data collected. The whole data collected with Brewer

Figure 3.4 – UVBrewer software showing UV-B data in January, the 8^{th}, 2008, a clear sky day.

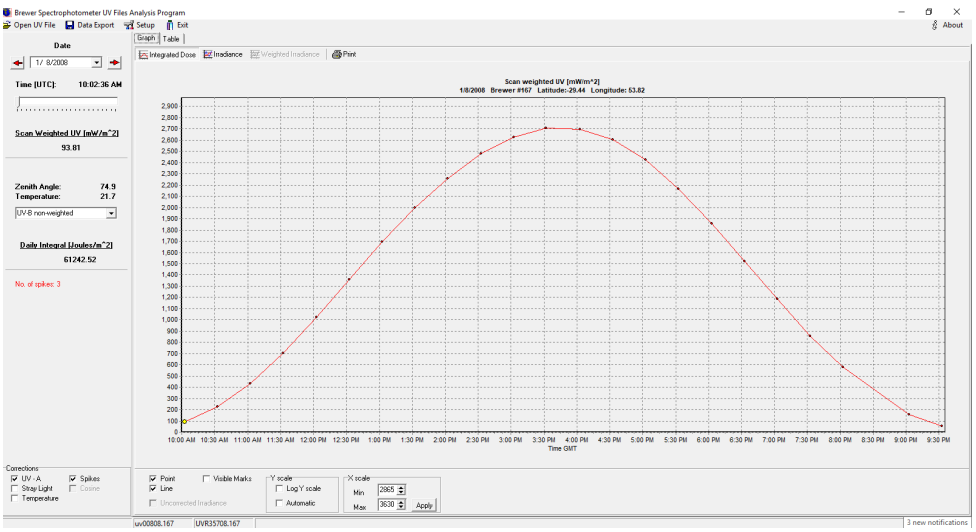

Source: Author.

Figure 3.5 – Daily distribution of scan weighted UV in December 7, 2008, with a cloudy period at 4 pm.

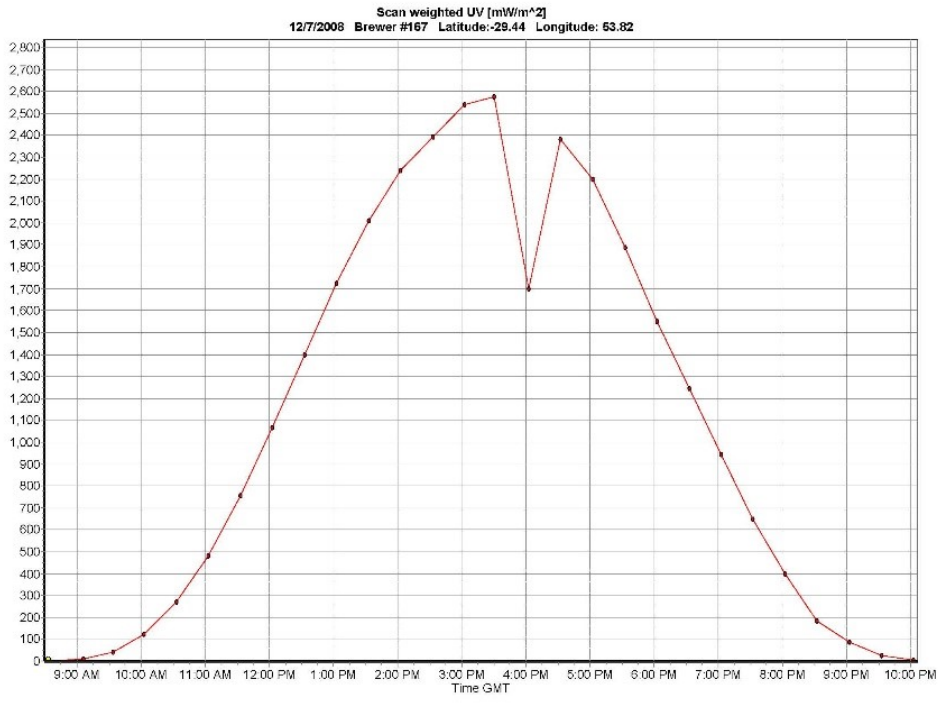

Source: Author.

in the period between 2005 and 2017 was checked and verified, being excluded days with errors of measurements. Measurements are done every 30 minutes, it starts close to 6 AM and it goes until 8 PM, local time. Data observation shows, in some days, a discrepancy in the number of measurements per day, so the number of counting may vary, reducing

the possibility of analysis of that specific solar day. Some days of measurements were not considered due to the lack of counting, containing only two of three points in some cases (SCI-TEC, 1999).

Thus, it was considered one data set of UV radiation containing all-sky conditions, which includes days with total open sky, open sky days with eventual occurrence of clouds sunny, partially cloudy and overcast days. This data set is referred as all-sky condition in data analysis. And a second data set was considered which contains only days with open sky conditions, this data set is referred as clear sky condition in this study.

Flowchart in Figure 3.6 shows all steps followed in data retrieval and data sets organization. Ultraviolet radiation analyzed in this study correspond to UV index, erythema dose, UV-B non-weighted and UV daily integral, from 2005 to 2017, from Brewer in all-sky conditions and, separately, in clear sky conditions. Clear sky days were selected based on the Gaussian form of irradiance curve and data from an All-Sky Camera (EKO Instruments).

The instrument is a digital camera composed by fish-eye lens and with a field of view of 180° , protected with a water prof box and heating system to protect from weather and temperature changes (LUIZ et al., 2018). The Total Sky Imager (TSI) , processes the image obtained and the ratio of cloud in the sky is estimated based on thin cover and opaque cover of clouds. Cloud fraction represents the cloud coverage, it is calculated with a software based on the image and type of cloud (SLATER; LONG; TOOMAN, 2001).

3.2.2.1 SELECTION OF DAYS WITH CLEAR SKY CONDITION

The selection of clear sky days was done manually by observing the irradiance curve produced in data processing phase of the study. The selection followed some criteria to analyze the curves and consider them as clear sky, such as the bell-shaped curve with a very smooth outline. Data selected was compared to cloud fraction values from an all-sky camera located on the same site, to verify the absence of clouds on the days studied.

It was developed a study using the TSI, positioned close to Brewer instrument intending to confirm the method used to select clear sky days from Brewer data set. It consists in an All-Sky Camera (EKO Instruments) and data used is cloud fraction, regarding to the cloud cover on the sky, as well as the treated images from the All-sky Camera of the corresponding days of the study.

It was selected a few days to make a comparison between cloud fraction from all-sky camera and UV index from Brewer spectrophotometer. The days chosen to be compared to cloud fraction and the images include days with clear sky condition and also cloudy days in order to verify the relation between cloud fraction and UV radiation, as cloud fraction increases due to the presence of clouds, UV radiation tends to decrease because of attenuation process caused by clouds. On the other hand, a clear sky day results in extremely

Figure 3.6 – Flowchart of data retrieved from Brewer spectrophotometer.

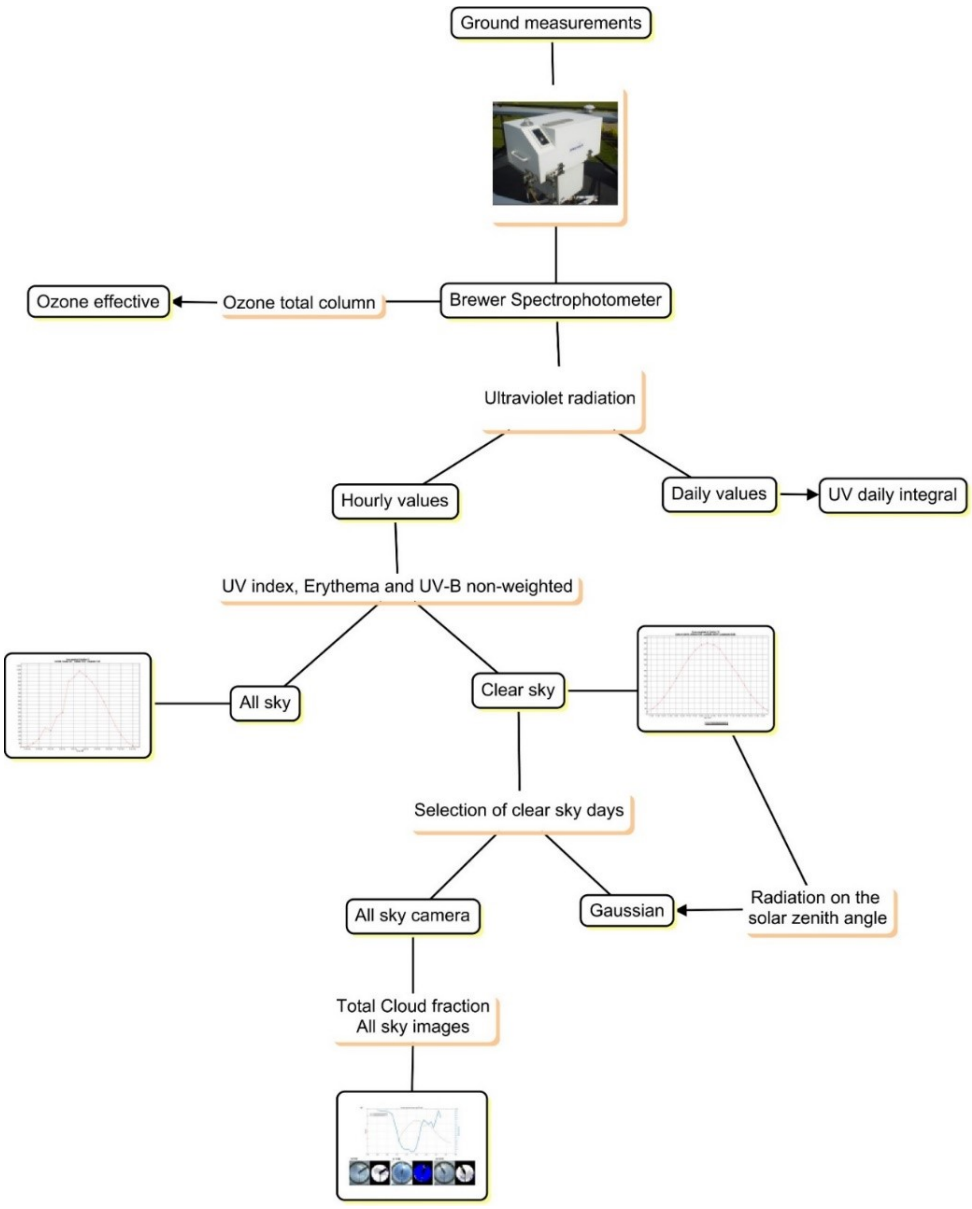

Source: Author.

low values of cloud fraction with values of UV index that increase along the day and decreases gradually after reaching its peak around noon, local time.

TSI is an instrument of atmospheric radiation measurement, the criteria applied in this study was the addition of cloud fraction thin and cloud fraction opaque, since it is the total of the two parameters that compose the cloud portion on the sky (Figure 3.7a) (SLATER; LONG; TOOMAN, 2001; KLEISS et al., 2018).

Thin cover is represented by the grey area of cloud cover meanwhile the whiter area represents the opaque ratio in the sky, as in the example shown in Figure 3.7a, on July 28, 2004, cloud fraction thin was 22.68% at 9:00 h, local time, and cloud fraction opaque was 72.61%, total of 95.30% of cloud cover on the sky (Figure 3.7b). Contrasting with the

Figure 3.7 – a) Total Cloud Fraction from TSI, in percentage and UV index from Brewer in July 28, 2004, Images from All-sky camera showing cloud cover at three different times during the day, b) 9 hours in the morning, c) 11:30 minutes and d) 14:15 minutes in the afternoon.

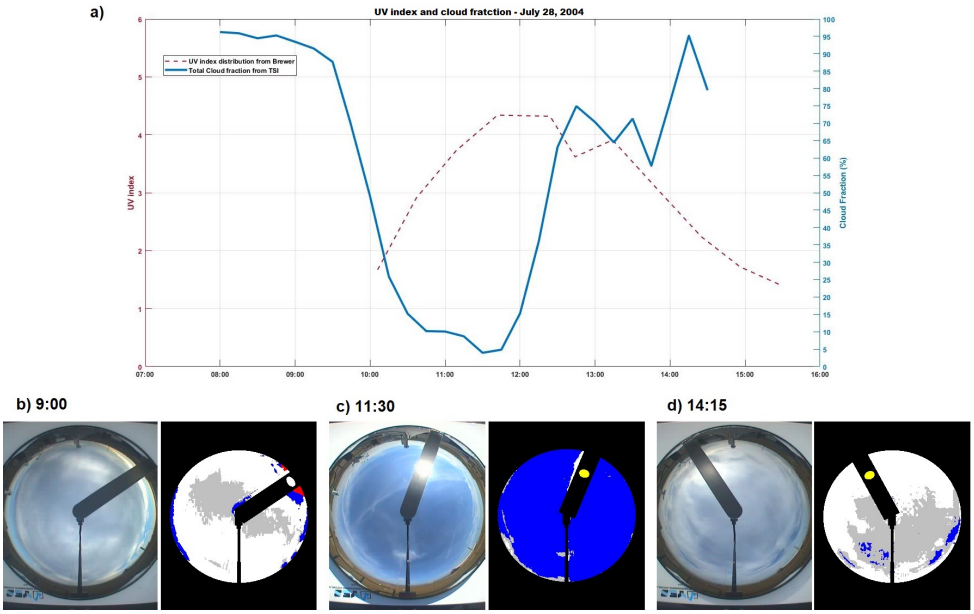

Source: Author.

condition at 11:30 min, local time, when cloud cover was 4.02% (cloud fraction thin was 2.92% and cloud fraction opaque was 1.10%, the blue clear area in Figure 3.7c is clear sky. It is clear the response of UV index (dashed line on the plot of Figure 3.7a) to the reduction of cloud cover, it rises proportionally to the reduction of cloud fraction. Cloud fraction thin and opaque at 14:15 were 41.51% and 55.59%, respectively, a total cloud fraction of 97.10%, a very high value, characterizing cloudiness only 2 hours and 45 minutes after a clear sky condition was observed. Cloud cover augment rapidly from noontime to the next hours of the afternoon and UV index gradually decreases, demonstrating the attenuation of radiation by clouds.

Total cloud fraction was matched with UV index to verify the method of selection of clear sky days. As an inquisitiveness manner cloud fraction was also matched with UV index to check the response of UV index distribution in cloudy days, since it is not a goal in this study.

The dates chosen were based on the availability of processed data of cloud fraction and treated image from All-Sky Camera Instrument and clear sky days pre-selected from Brewer Spectrophotometer data series. It was selected from July 21, 2004 to July 25, 2004. UV index distribution related to cloud fraction on these days can be observed on Figures from 3.8a-e to 3.12 a-e as well as treated images from all-sky camera in determined hours of the day. The time was adjusted to the local time, since the measurements from Brewer and from All-Sky Camera are done in GMT time, that is plus 3 hours on the original time

zone.

The images were selected based on the time when it was most clear the absence or presence of clouds, depending on the day of example, since days July 22 and 23, 2004 are representing cloudy days. Figures 3.9 and 3.10 are well representing the influence of clouds on UV index levels, it is highly important to mention that those specific days were not included in clear sky data set, though. They are being used as an example of how a day with the presence of clouds would, graphically, appear to be as well as how clouds are seen on the treated image of All-Sky Camera.

Period of year of the days selected is winter time in the region of study and specifically when the lowest UV index are registered because insolation is less intense and also the period of sunlight is shorter. This period of the year the instrument runs with lower zenith angles, generating less points of UV data from Brewer along the days, even-though it is clear the absence of clouds on the days of July 21, 24 and 25, 2004, as it can be seen in the Figures 3.8, 3.11 and 3.12. UV index reaches a maximum of almost 5, it is a moderate level of UV index on those days.

Figure 3.8a contains the UV index on red dashed curve and total cloud fraction calculated represented by the blue line. Images on Figure 3.8b-e show the clear sky of the day. Approximately at 14:30 minutes there is a little bump on total cloud fraction line, which corresponds to 2.57% of cloud fraction, at 15h a similar bump occurs, corresponding to 2.70% of total cloud fraction, it is possible to observe in Figure 3.8d, the small percentage of total cloud fraction represented in the image. The impact of that on the UV index is very slightly on the plot (Figure 3.8a) and not significant enough to interfere on UV index measurement.

Figure 3.8 – a) Total Cloud Fraction from TSI, in percentage and UV index from Brewer on July 21, 2004, Images from All-sky camera showing cloud cover at four different times during the day, b) 9 hours in the morning, c) 12 hours, d) 15 hours in the afternoon and e) 17 hours.

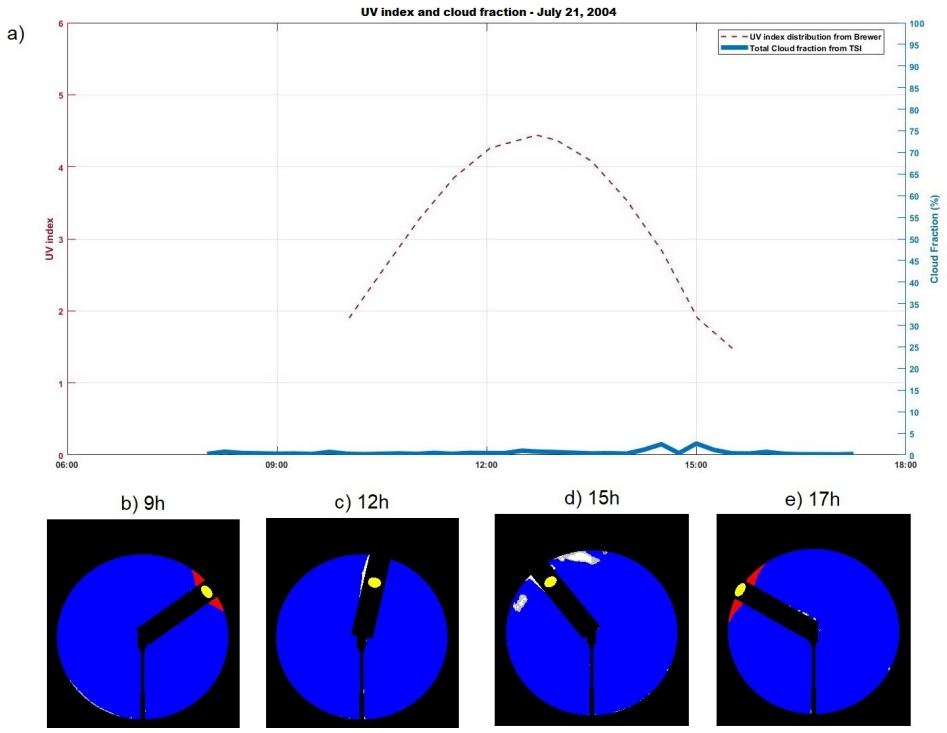

Source: Author.

The plot of UV index and total cloud fraction of July 22, 2004 (Figure 3.9a) one can observe cloud fraction reaching 50% at 9h (Figure 3.9b, observing the cloud cover at this time it was mostly composed by cloud fraction thin, represented by gray area in the image. Later in the morning, at 11h total cloud fraction reached around 90%. The UV index tends to increase as the total cloud fraction decreases around noon time (Figure 3.9d) and at 17h total cloud fraction is 78%, which apparently is composed more by cloud fraction opaque than thin (Figure 3.9e).

Figure 3.9 – a) Total Cloud Fraction from TSI, in percentage and UV index from Brewer in July 22, 2004, Images from All-sky camera showing cloud cover at four different times during the day, b) 9 hours in the morning, c) 11 hours showing cloudiness and right after at d) 12 hours almost clear sky was captured, and e) 17 hours in the afternoon.

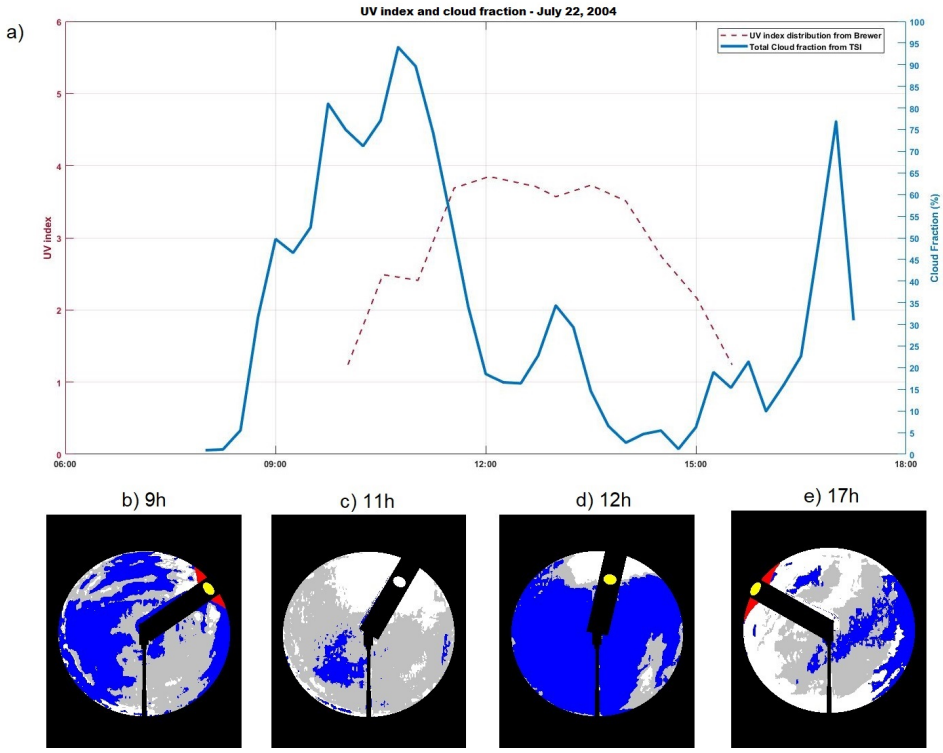

Source: Author.

July 23, 2004 was also considered a cloudy day (Figure 3.10a-e) the images show low total cloud fraction mostly of the morning, reaching around 16% late in the morning (Figure 3.10c. Even though it does not cause a great impact on UV index, Figure 3.10a, the image on Figure 17c shows significant cloud cover, mostly of it appear to be cloud factor thin, then it consists in a day with cloud condition. Which is confirmed approximately 15h, when it is visible the influence of clouds on UV index, as total cloud fraction increases, reaching its maximum at that day, 68% causing some peaks on UV index curve (Figure 3.10a and d). Figure 3.10d shows slightly less cloud cover than Figure 3.10d when total cloud fraction was 63%.

Figure 3.10 – a) Total Cloud Fraction from TSI, in percentage and UV index from Brewer on July 23, 2004, Images from All-sky camera showing cloud cover at four different times during the day, b) 11 hours in the morning, c) 12 hours, d) 15 hours and e) 17 hours.

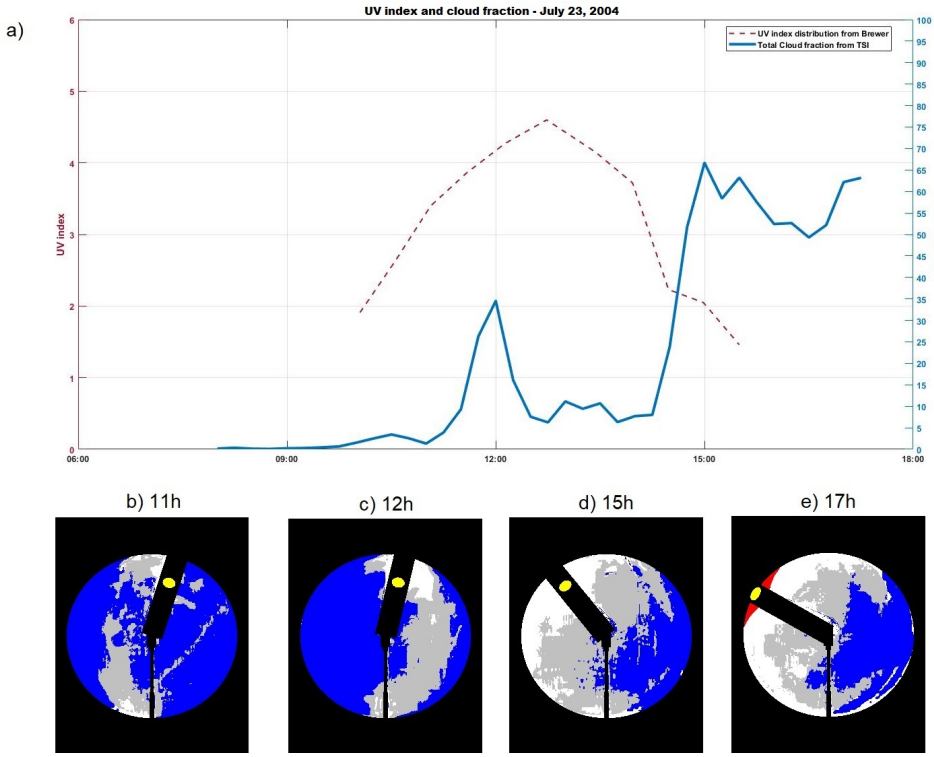

Source: Author.

Identified as a clear sky day, July 24, 2004 (Figure 3.11a) reached its maximum total cloud fraction in 2.9% at 8:15 minutes, as it can be observed in Figure 3.11b. Even though there is not a UV index measure at this time, at 11:00 hours total cloud fraction reached 1.66%, while the UV index was 4.08. Based on the previous and following values of UV index, and on the comparison of the images from All-sky camera in Figures 3.11b and c, it was concluded that UV index wasn't affected by this amount of total cloud fraction. Figure 3.11d-e confirm clear sky condition on the rest of the day.

Figure 3.11 – Cloud fraction and UV index on July 24, 2004.

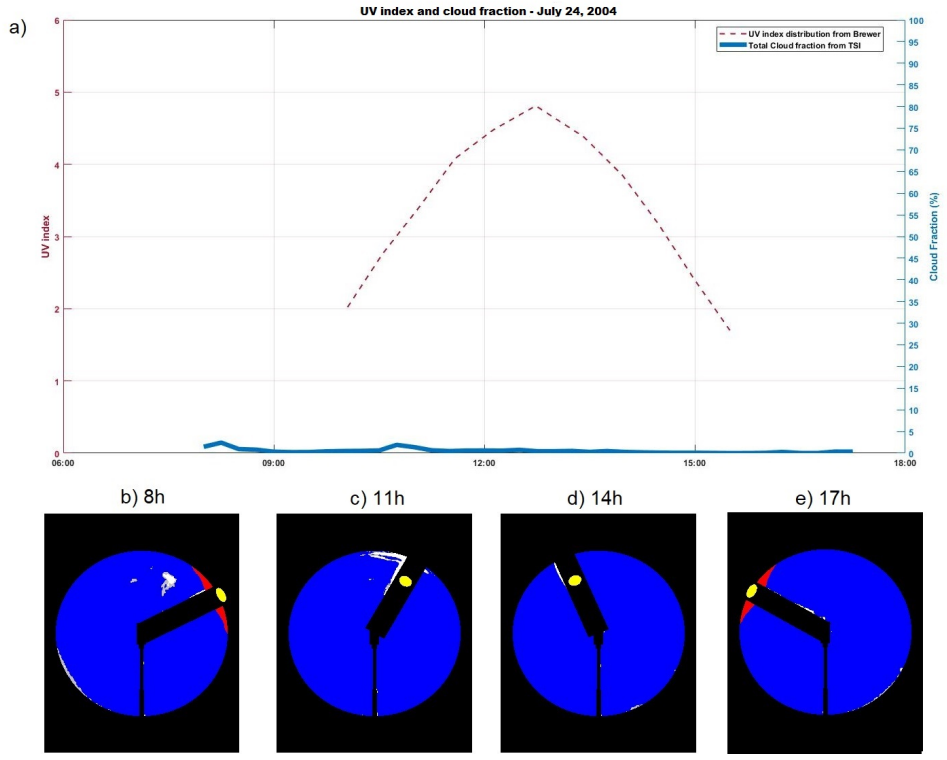

Source: Author.

Total cloud fraction of July 25, 2004 was always under 1%, UV index curve represents a day with clear sky condition, reaching its maximum in almost 5 (Figure 3.12a), a very typical behavior of UV during this period of year, in this region. Figure 3.12b-c represent the ideal clear sky day.

Figure 3.12 – Cloud fraction and UV index on July 25, 2004.

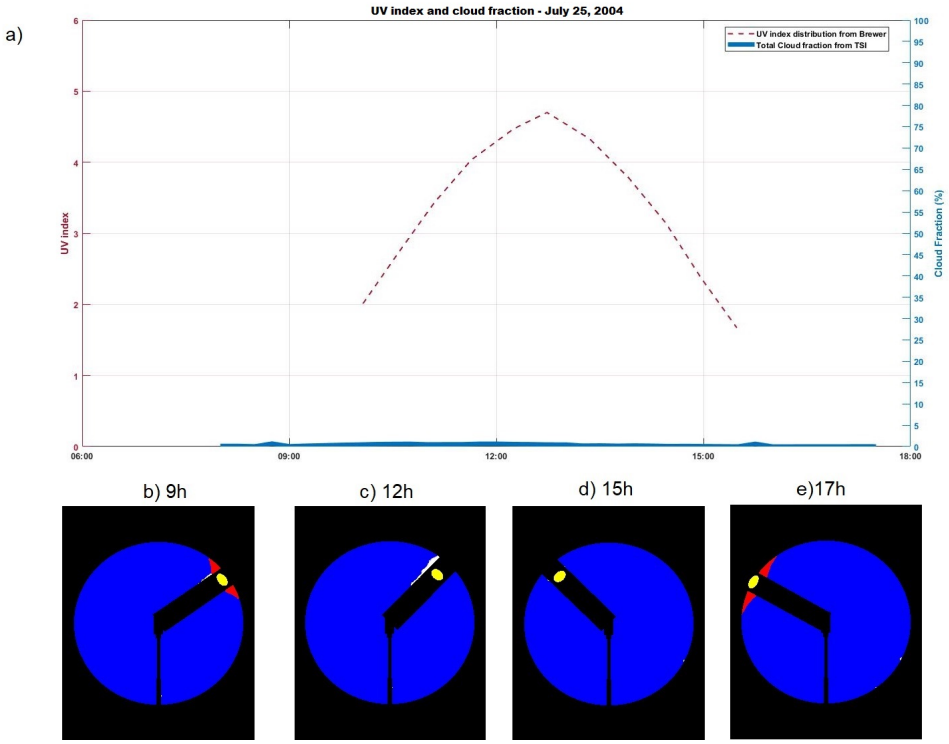

Source: Author.

The cloud fraction analysis in respect to the UV index behavior confirms that cloud cover influences UV index, especially on what was mostly observed in this study, it impacts the smoothness of UV index curve, causing spikes and bumps, interfering in the ideal Gaussian form of UV index curve. It is relevant to mention that the type of cloud influences on the severity of those spikes, depending on the type of clouds, UV radiation can even be increased because of scattering. Most important, high percentages of cloud fraction do not indicate that the sun is covered by clouds, since cloud fraction represents the presence of clouds in the sky which do not mean that the sun is covered by them. That is why in some cases high percentages of cloud fraction did not interfere significantly on UV index curve. Based on that it was established a maximum of total cloud fraction of 5% to be considered a day with clear sky condition.

3.3 OZONE MONITORING INSTRUMENT (OMI)

Ozone Monitoring Instrument aboard of satellite ERS-2, launched in 2004 to continue the measurements done previously with satellite TOMS (Total Ozone Mapping Spectrometer), when in 2005 ended its measurements. The satellite is a nadir-viewing spectrometer with 2600 km wide viewing swath which provides global coverage in 14 orbits, Earth is

observed in 740 wavelength bands along the satellite route.

OMI sensor is equipped to measure and collect data regarding to ozone, aerosol and other gases in the atmosphere, it measures ozone total quantities through the analysis of the back-scattered solar radiation, it also measures solar reflected light in a selected range of the ultraviolet and visible spectrum. The sensor is 13 $\times$ 25 km special resolution with two ultraviolet bands named UV-1 (270 to 314 nm) with a spectral resolution of 0,45 nm and UV-2 (306 to 380 nm) with spectral resolution of 1 nm.

The data was downloaded from Giovanni platform specifically for the site where ground-based data was collected, on the coordinates 29.4°S, 53.8°W and grid 1° $\times$ 1°, and the data set is from the year of 2004 to 2017 (OMI, 2002; GIOVANNI, 2017; TANSKANEN et al., 2006).

3.4 DATA ANALYSIS

3.4.1 Comparison analysis between ground-based and satellite data

The comparison study was carried between ground and satellite data of UV index on clear sky days, from 2005 to 2017. Correlation of the two data sets is important to verify the similarities between them, as in Equation 3.1 through the calculation of correlation coefficient (r). The differences between data sets is determined with the daily bias (Equation 3.2). The difference among the values from ground and satellite is the root means square error (RMSE) seen in Equation 3.3. In order to ensure a good result, it was calculated the mean absolute bias error (Equation 3.4). The dispersion of Bias was obtained through standard deviation, in Equation 3.5.

$$r = \frac{\sum_m \sum_n (Bre_{mn} - MeanBre)(OMI_{mn} - MeanOMI)}{\sqrt{(\sum_m \sum_n (Bre_{mn} - MeanBre)^2 (\sum_m \sum_n (OMI_{mn} - MeanOMI)^2)}} \tag{3.1}$$

$$Bias(\%) = \frac{100}{N} \sum_{i=1}^{N} \frac{OMI - Bre}{Bre} \tag{3.2}$$

$$RMSE = \sqrt{\frac{1}{N-1} \sum_{i=1}^{N} (OMI - Bre)^2} \tag{3.3}$$

$$MABE = \frac{100}{N} \sum_{i=1}^{N} \sum_{i=1}^{N} \frac{|OMI - Bre|}{Bre} \tag{3.4}$$

$$Standard \quad Deviation = \sqrt{\frac{1}{N-1}\sum_{i=1}^{N}((OMI - Bre) - Bias)^2} \tag{3.5}$$

3.4.2 Climatology of UV data from Brewer spectrophotometer

All data extracted from Brewers software regarding to UV radiation were studied through the analysis of the climatology of the data series. The monthly and daily means were calculated for both all-sky conditions and clear sky conditions data sets, besides that, the daily means of each season of the year was calculated. The means were calculated with Equation 3.6, the standard deviation was also calculated (Equation 3.7).

$$\mu = \frac{1}{N}\sum_{i=1}^{N} UVindex_i \tag{3.6}$$

$$Std = \sqrt{\frac{1}{N-1}\sum_{i=1}^{N} |UVindex_i - \mu|^2} \tag{3.7}$$

The study of inter-annual variations of UV radiation was done in order to see different influences acting on the region besides seasonal ones. Wavelet analysis was applied and it is required a complete filled data series with continuous measures along the period therefore UV index data set was rebuilt using the same parameter measured with OMI sensor. First of all, maximum UV index measured in days with clear sky condition were selected, then, the random gaps in time series were completed with UV index from satellite, also measured in clear sky days. Eventually there were days with missing data in both time series, in those cases, the mean was calculated among the previous and next days of measurements in order to complete the continuous data series. Reconstructed data series Brewer-OMI started in 2005 until 2017.

The anomaly was obtained by the subtraction of the monthly climatological mean from the daily value of UV index. The wavelet transformed Morlet was applied to the anomaly data series. The Morlet method of transformed wave consists in a plane wave modulated by a Gaussian function, represented by Equation 3.8 (TORRENCE; COMPO, 1998),

$$\psi_0(\eta) = \pi_4^1 e^{i\omega_0\eta} e^{\frac{-\eta^2}{2}} \tag{3.8}$$

where: ω_0 is the non-dimensional frequency; η is the non-dimensional time parameter.

Considering the discrete time series (Xn), with a fixed time spacing (Δt) and $n = 0, ..., N-1$, the continuous wavelet transform is in Equation 3.9, where ($*$) is the complex

conjugate and s is the period (wavelet scale). The global wavelet spectrum (Equation 3.10) allows to calculate the unbiased estimation of the true power spectrum of the time series, through the calculation of the average wavelet spectrum over a period.

$$W_n(s) = \sum_{n'=0}^{N-1} X_n \psi * \left[\frac{(n'-n)\Delta t}{s} \right] \tag{3.9}$$

$$W^2(s) = \frac{1}{N} \sum_{n=0}^{N-1} |W_n(s)| \tag{3.10}$$

Wavelet represents functions in different scales and time (DAUBECHIES, 1992). The wavelet is composed by the power spectrum, where the edges are closed by a U curve called cone of influence, where there is a 95% confidence level. The global wavelet spectrum contains the most significant values and on the right side of the dotted line, indicates 95% confidence level, being statistically significant the curve that passes this line. In order to determine the measure of relative power for the anomaly time series, wavelet power spectrum was normalized with $\frac{|W_n(s)|^2}{\sigma^2}$.

3.4.3 Events of secondary effects of Antarctic ozone hole

Events of secondary effects of ozone hole are characterized by ozone-poor air masses that are released from the Antarctic ozone hole and end up reaching mid-latitude regions. It is known that those masses can reach south American continent, impacting the region in south Brazil, where the present study was carried (KIRCHHOFF et al., 1996).

Previously to the study of events of secondary effects of Antarctic ozone hole, an analysis of correlation was made between UV radiation data (Erythema dose) from Brewer and effective ozone. It accounts for the attenuation of solar radiation on the atmosphere because it considers the solar zenith angle at the time of measurement. It was obtained with the multiplication of ozone total column values by the secant of solar zenith angle (θ) at the time of measurement of ozone (BERTAGNOLLI et al., 2005).

A methodology for identification of the events of secondary effects of Antarctic ozone hole used in the present study was previously described by Peres et al. (2019), and Bittencourt et al. (2018b). A total of 58 events were identified by Peres et al. (2016) between 2005 and 2014, and later 34 events were identified by Bittencourt et al. (2018b), between 2006 and 2016. A specific event, on October 2016, was reported by Bittencourt et al. (2018a) in a study on the behavior of the dynamics of troposphere and stratosphere during the occurrence of event. It was conducted using total ozone column measured with same instrument and site of the present research.

Overall the events of secondary effects of Antarctic ozone hole were identified through

analysis of ozone total column, potential vorticity fields and backward trajectories of air masses, from HYSPLIT model (ROLPH; STEIN; STUNDER, 2017). Firstly, days when the ozone total column daily mean was lower than the climatological mean of the month, were identified. As a second step to obtain the absolute potential vorticity in isentropic surfaces of the region, confirming the occurrence of event. The reason why this is done is because potential vorticity acts as air-mass tracker, where potential temperature is conserved and used as horizontal coordinate (HOSKINS; MCINTYRE; ROBERTSON, 1985).

Then, it was determined if the origin of the air-mass, through the potential vorticity field in isentropic surfaces. In order to analyze the stratospheric dynamics during events, these fields help to identify the origin of the air mass where when there is an increase in potential vorticity the origin is polar and the opposite when there is a decrease in potential vorticity the origin is equatorial. Stratospheric fields in four different potential temperatures (475 K, 530 K, 600 K and 700 K) were obtained using daily mean data from ECMWF (SEMANE et al., 2006). Finally, with all events identified, meteorological fields of troposphere dynamics were done in order to observe its behavior prior, during and days after the events (BITTENCOURT et al., 2018b).

Usually the events tend to be persistent for a couple of days after its arrival on the region, until ozone total column is recovered and UV radiation reduces. Besides that, in some events it was cloudy at day of event, shading the UV radiation increase at this day, for this reason, in some cases, it was selected a day after the day of event when UV index reached higher values, instead of the specific first day of event.

A total of 10 events were selected to be studied in this research considering availability of UV radiation data from Brewer. The events occurred between 2005 and 2016, being seven events with its first day happening with a clear sky condition and seven events with cloudy sky condition in its first day.

Ozone total column and UV index from Brewer spectrophotometer were used in this study. Eventual gaps in ozone data set was filled using data retrieved from OMI sensor. With daily values of ozone total column and maximum daily UV index from Brewer, the climatological monthly mean was obtained for both ozone and UV index. Those daily values of ozone total column and UV index were plotted considering 10 days before and 10 days after the day of event, in order to visualize UV index response to the decrease in ozone total column. Satellite images of each event studied were included with the intention to observe cloud cover in the region. Satellite images GOES 13 are from thermal infrared channel, it helps in analysis of troposphere, identifying the systems influencing the region of study (CPTEC, 2017).

4 RESULTS AND DISCUSSION

4.1 UV INDEX MEASUREMENTS

Ground and satellite observations of UV radiation are extremely important to be studied. Each one with its methods of measurement and collection of data, provide an overview of solar UV radiation reaching the surface. A deeper analysis of those data can lead to a better understanding of the energy budget on Earth and more specifically, how UV radiation behaves and reacts to different types of interference such as seasonal changes, action of different circulations in the atmosphere, changes in ozone total column over the region, even the rain regimes can cause great impact on the irradiance reaching the surface.

Satellite overpass time provides one measurement per day, it reads back scattered radiation which accounts with cloud cover and also have contribution from aerosol load, surface and topography of the region (DAMIANI et al., 2014). While the surface monitoring instrument used in this study provides measures of UV radiation every 30 minutes and also accounts with a diffuser to read UV directly coming from sun beam, which also scatters from clouds at all angles (PARTOSOEBROTO, 2014). Therefore, it is highly relevant to consider both ground and satellite measurements.

UV index single measurements per day, from OMI can be observed in Figure 4.1, represented by orange dots and UV index from Brewer, all measurements per day, in blue dots. Plot a, contains measures in all-sky conditions and plot b measures on clear sky condition. Visually, they both present a very similar pattern considering UV index, when overlapped. It is evident the gaps along the years on Brewer data, specially between 2010 and 2011, when the equipment underwent maintenance, even though it is very clear the annual periodicity and consistency between both is very apparent.

Figure 4.1 – Comparison of UV index daily measurements from Brewer spectrometer (blue dots) and OMI (orange dots) of all-sky (a) and clear sky conditions (b).

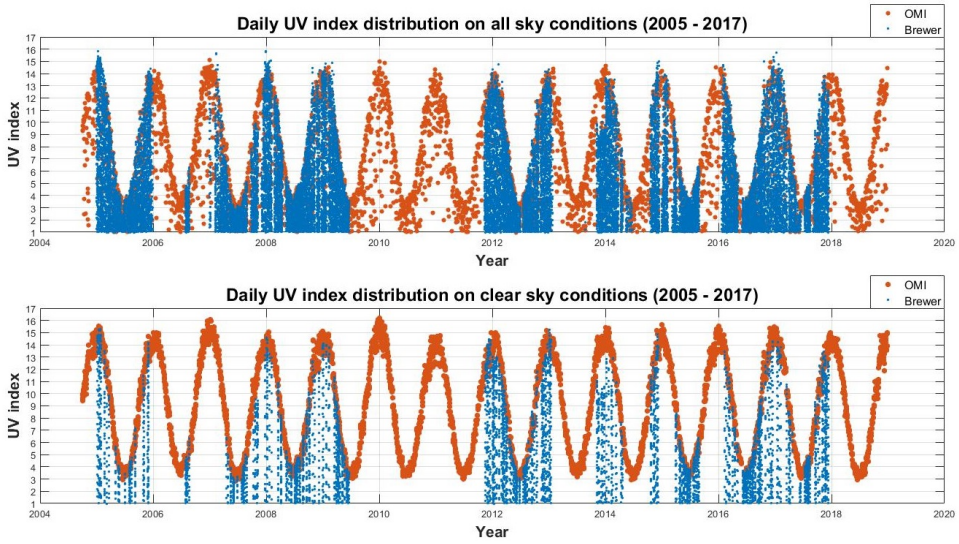

Source: Author.

Correlation between the two sources of measurements, satellite and ground-based is essential in order to validate this data, so for this analysis it was considered clear sky days and only one measure per day around noon time, along all the period between 2005 to 2017. In order to perform the correlation analysis, it was necessary that both data series consisted of the same length of measures.

UV index measures retrieved from OMI satellite contains more days of measurements than data set from Brewer, so it was considered to be more coherent to select all days of measurement that are in common for both sources of data (Figure 4.2, plot a). Therefore, the gaps observed on the UV distribution from Brewer and OMI are due to the fact that it was only considered the days that contained measures from both, satellite and Brewer of UV index, in this analysis.

Figure 4.2 – Maximum UV index daily data distribution from Brewer and from OMI overlaid, measured around noon time, from 2005 to 2017 (a). Scatterplot of maximum daily UV index measured with Brewer and OMI (b). Bias distribution showing the main difference between UV index from Brewer and OMI and correlation (c).

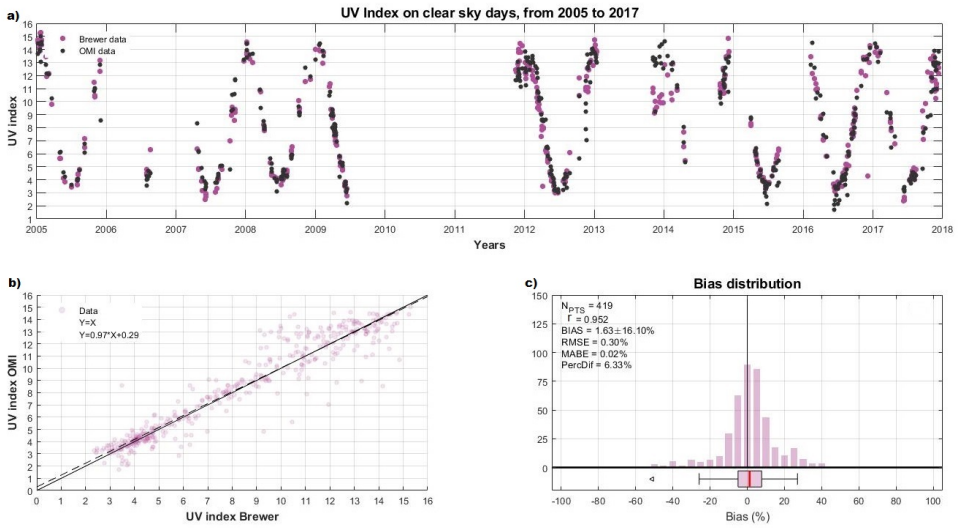

Source: Author.

Linear regression between UV index values from OMI and Brewer resulted in a good correlation with correlation coefficient (R) of 0.95 (plot b). The comparison resulted in a slightly overestimation of OMI over Brewer instrument data. MABE values indicate that the difference between daily measurements are small, 0.02% and RMSE was 0.30%. It means a positive correlation was found and the data-set does not vary much when compared to each other (plot c). Good pattern agreement and similar correlation results were also found by Cadet et al. (2017) in a study developed in South Africa, comparing UV index from OMI and surface instrument (UV biometers) also considering only clear sky days, in six different sites in South Africa.

Many authors have reported the overestimation of satellite-derived UV measurements when compared to ground-based data. The factors influencing satellite and surface measurements include aerosol load in the atmosphere, height of ground site, and cloud cover at the time of measurement. Antón et al. (2010) reported that OMI overestimated Brewer measurements near 12% of UV (324 nm) and more than 14% (305 nm) and between 8 and 14% for all-sky conditions, in a study developed in the south of Spain. Previously, the same author, Antón et al. (2007), in the same site in south of Spain, used satellite-derived data from TOMS and concluded that overestimated Brewer measurements of Erythemal UV irradiance in 12% in clear sky days (WANG et al., 2014) (SCI-TEC, 2019).

The study developed by Ialongo, Casale & Siani (2008), in Italy, OMI overestimated all surface equipment studied, including Brewer in almost 20%. The same was reported by Kazadzis et al. (2009), in a study developed in Greece, where OMI also overestimated Brewer measurements of UV irradiance in 30%, 17% and 13% for wavelengths 305, 324

and 380 nm, respectively (MCGEE; JR, 1987; MOLINA; MOLINA, 1986).

Comparison study shows coherent result between both sources of UV index data, it also shows the particularities of each source of data. Accordingly to other studies satellite measures tends to overestimate measures from ground instruments. Even though there was a slightly overestimation of UV index from OMI over Brewer instrument, the results obtained here were considered adequate for the region of study and suitable with other similar studies.

4.2 CLIMATOLOGY ANALYSIS OF UV RADIATION DATA FROM BREWER SPECTROPHOTOMETER

4.2.1 Seasonal variation of UV index

Measures of UV radiation collected between 2005 and 2017 with Brewer spectrophotometer were processed using biological filter and UV index was obtained. Figure 4.3, plot a, contains the daily distribution of UV index along the period of study. This data corresponds to measures taken every 30 minutes, starting around 6 hours in the morning until around 9 hours at night.

All measures were accounted to calculate daily and climatology monthly averages, also seen in the plot b and c, respectively, in the same Figure. Daily mean shows the average UV index per hour of day and the datas standard deviation with a wide range. Midday is the hour of day when sun is at highest in the sky, reaching its peak around 6 in the UV index scale, high value (>6 and <7). The maximum UV index registered each hour of day along the period were included in the daily mean plot so it is possible to see they reach extreme values (>11), differently from what it is seen in the means where UV index is lower.

Maximum average of UV index is reached during summer time when observing average UV index by month, Figure 4.3, plot b. The climatology monthly mean was calculated considering the mean by hour (plot c), is distributed along the months, which were adapted for better visualization of UV index during the year. UV index is represented in color bar, showing a maximum of 12 (extreme >11), mainly between December and end of January. Months preceding and following the summer it varies between very high (>8 and <10) and high. During winter in south hemisphere monthly mean shows moderate (>3 and <5) UV index for the latitude of the Southern Space Observatory, 30^{o}S.

Figure 4.3 – Daily data distribution of UV index on all-sky condition, 2005 to 2017 (a). UV index distribution with all measures of UV index (blue dots), in all-sky conditions, from 2005 to 2017. Daily mean of UV index (b), in yellow line, shows the mean of all measures in all-sky conditions of UV index per hour of day. Standard deviation in dashed lines, and the maximum UV index registered per hour of day are represented in purple diamonds. Monthly climatology of all measures in all-sky conditions are distributed along the months of the year per hour of day (c), the plot was adapted for better visualization of UV index which is represented in color bar.

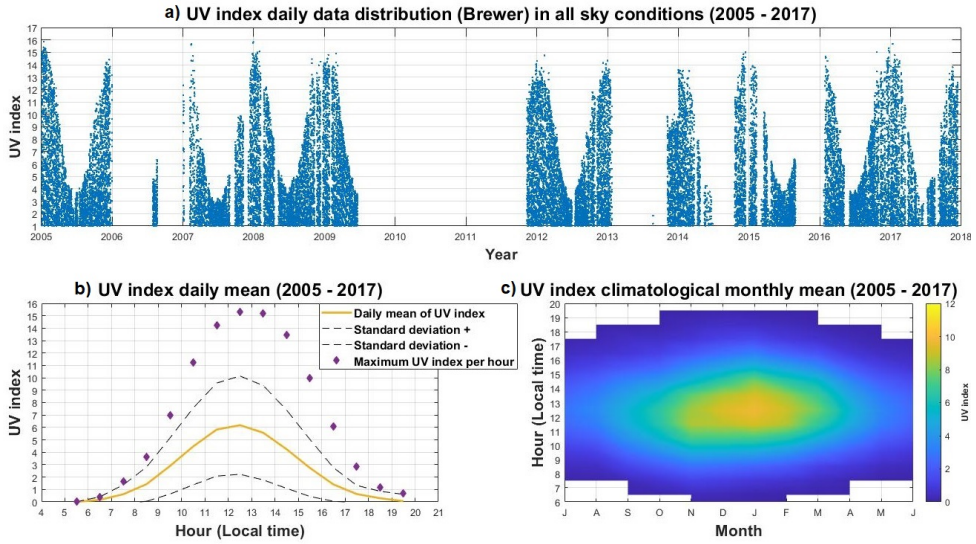

Source: Author.

Due to the strong seasonal behavior of UV radiation and the fact the four seasons are well defined in the region, it was considered important to calculate the daily average UV index per season of the year. It is seen in Figure 4.4 daily mean of UV index in summer (plot a), considered December, January and February, months with the most intense UV radiation on the region, followed by spring (plot d) (September, October and November), with a daily mean of 7 (high in the scale). Plot c, winter season daily mean (June, July and August) months with the lowest UV radiation intensity and autumn (March, April and May), in plot b, showing daily mean reaches 6, also high in the scale. While the daily averages vary between moderate and very high UV index, maximum values of UV index were included showing mostly of the year it reaches extreme, with exception only of winter season.

Seasonal variations of UV radiation and mainly the characteristic of annual cycle observed, is due to the radiation intensity on the region, which besides many attenuating factors, also varies with geographic location (30° South) as the latitude of the site, time of day and the season because it reflects on the solar zenith angle. The higher the solar zenith angle the lower is the UV radiation intensity. Aerosols may reduce UV radiation intensity up to 15% in urban areas and locals with high pollution levels (FIOLETOV; KERR; FERGUSSON, 2010; PREEZ et al., 2021), although the site of study is located in a rural

Figure 4.4 – Daily mean of UV index on all-sky condition (yellow line) per season, summer (a), autumn (b), winter (c) and spring (d). Standard deviation is the dashed line and maximum UV index per hour of day is indicated with purple diamonds. The daily means are from all measures in all-sky conditions from 2005 to 2017.

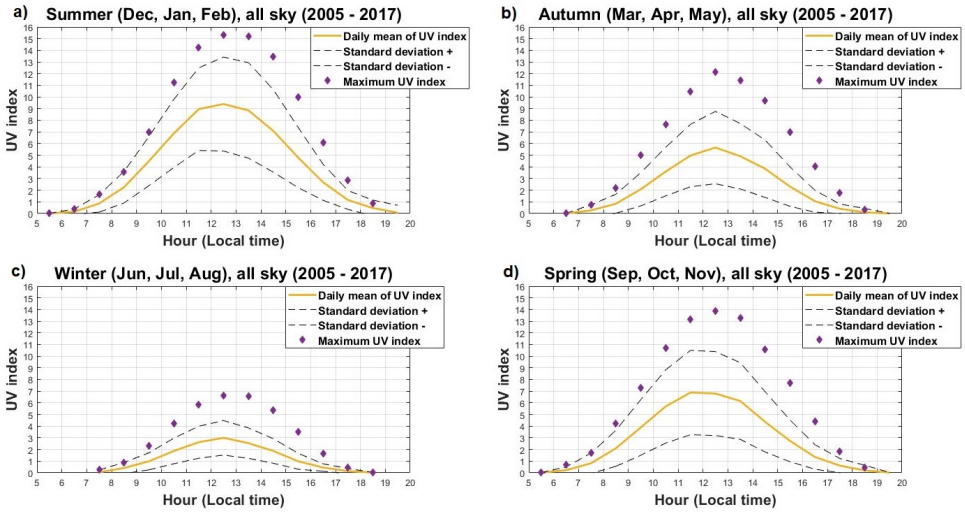

Source: Author.

area with clean background atmosphere although close to urban sites, aerosol load was not accounted in this research, differently to cloud effects.

Cloud effect can have a very significant role on attenuation of UV radiation (WEIHS et al., 2008). Depending on the cloud formation, such as stratified are homogeneous with uniform and sheet-like appearance, formed by the cooling of a stable layer, can reduce UV radiation in 50% when compared to a day with clear sky. Rain-cloud as cumulonimbus might reduce UV radiation intensity on the surface to practically zero (CORRÊA, 2015). Even though the exactly quantification of its effects on UV radiation is still not confirmed because of the dynamic variation in cloud formation and difficulty in predict its composition, there is evidence that suggests surface equipment are more accurate in cloud effects measures than satellite retrieved data (MCKENZIE et al., 1998).

So that it was considered important to study days with clear sky conditions separately in this research. Figure 4.5 shows UV index distribution from days with clear sky conditions (plot a), it includes every measure collected along the days selected. They were all included in the data set of all-sky conditions, described previously. However, in this part of study, they are being seen separately, that is why they present less days of measures and the same seasonal behavior including extreme values, which is characteristic of days with clear sky conditions since there is no attenuation of UV radiation by cloud effects.

Figure 4.5 – Daily data distribution of UV index on clear-sky condition, 2005 to 2017 (a). UV index distribution with all measures of UV index (blue dots), in clear-sky conditions, from 2005 to 2017. Daily mean of UV index (b), in yellow line, shows the mean of all measures in clear-sky conditions of UV index per hour of day. Standard deviation in dashed lines, and the maximum UV index registered per hour of day are represented in purple diamonds. Monthly climatology of all measures in clear-sky conditions are distributed along the months of the year per hour of day (c), the plot was adapted for better visualization of UV index which is represented in color bar.

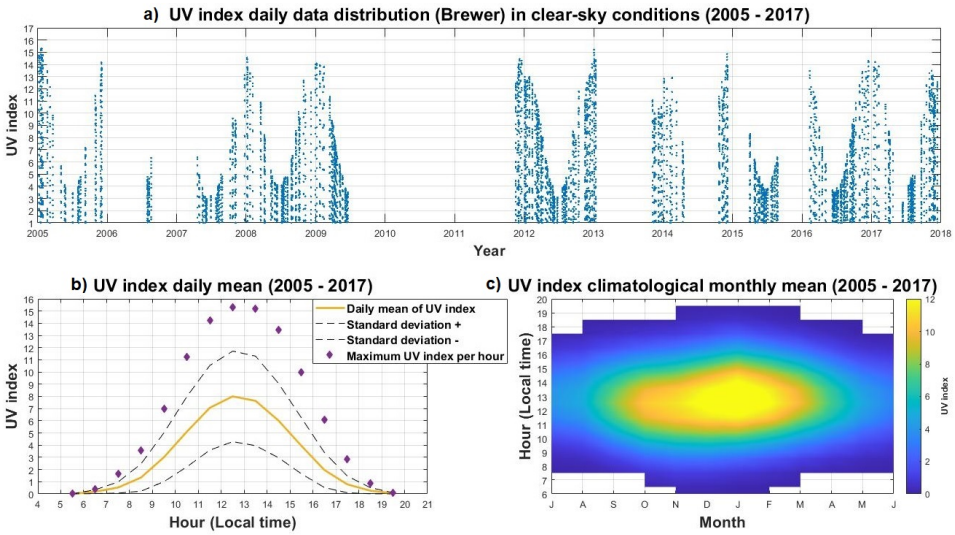

Source: Author.

Daily mean of UV index measures on clear sky conditions (plot b) are higher than considering all-sky conditions, its peak around noon time reached 8 (very high UV index). Standard deviation in clear sky conditions varies slightly less than in all-sky conditions. Maximum UV index per hour of day are the same seen in all-sky conditions, they correspond to days with clear sky condition. An important observation regarding maximum UV index per hour of day is that between 9 and 10 hours in the morning until 17 hours in the afternoon it varies from high to extreme, in the scale of UV index, so mostly of the day it is necessary to have precautions with sun exposure.

Hourly average UV index calculated by month of year, seen in the plot c of Figure 4.5, shows higher mean of UV index along the months than all-sky conditions. Extreme UV index occur in November, previous to summer season and go until March of next years, already autumn season. Very high UV index is predominant between September and early October and between March and late April. Between June and August, it appears that high UV index means are more constant.

Looking at daily means of UV index in clear sky condition calculated for each season of year (Figure 4.6), it is evident the higher intensity of UV radiation during the summer and spring seasons. Daily means of every season are higher than in all-sky condition, being 44% higher in summer season, almost 43% higher in spring season and 16 and 33% higher in autumn and winter seasons, respectively. As well as it is observed standard

deviation varies much less in clear sky conditions. Maximum UV index registered per hour of day remains the same. An alerting finding is that mostly of the year, nine months to be exactly, UV index reached extreme levels, rising the concern of measures of protection to sun exposure, not only in summer season.

Figure 4.6 – Daily mean of UV index on clear-sky condition (yellow line) per season, summer (a), autumn (b), winter (c) and spring (d). Standard deviation is the dashed line and maximum UV index per hour of day is indicated with purple diamonds. The daily means are from all measures in clear-sky conditions from 2005 to 2017.

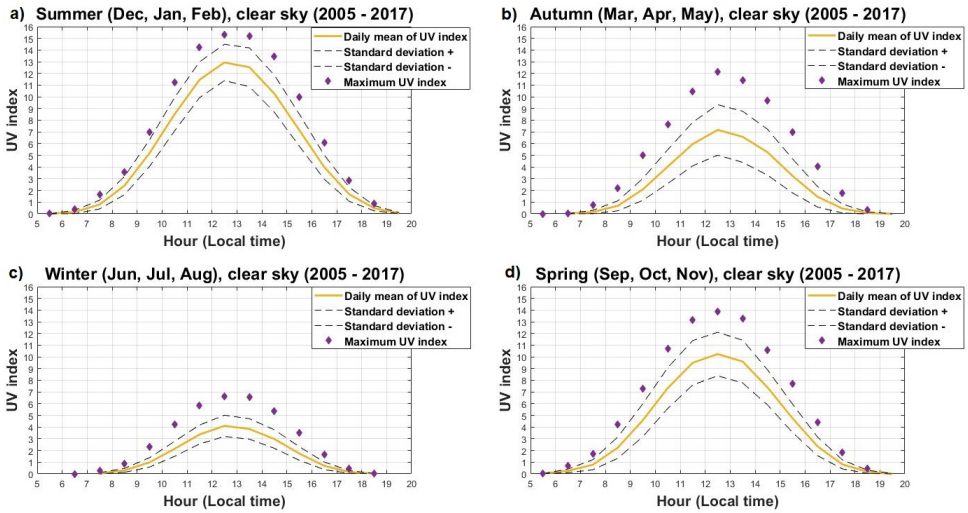

Source: Author.

The complete data set of UV index from Brewer contains one measurement every 30 minutes along the day and, in clear-sky condition, highest levels tend to be registered around noon time because the sun is the highest in the sky. In all-sky condition the highest UV index can be at any time of the day due to the oscillation of radiation with cloud attenuation. Therefore, it was selected the maximum UV index per day for both data sets, all-sky and clear sky conditions. The period of twelve years studied accounts with 2460 days with measures of all-sky conditions and from those, 423 days were considered days with clear sky conditions. Based on that, it was calculated the percentage frequency of days that registered each level of UV index, according with the scale. Figure 4.7 shows the percentage distribution along the year for all-sky and clear sky conditions.

UV index varies more along the months in days with all-sky conditions than in clear sky conditions, when it is predominant higher UV index, as expected. In both all-sky and clear conditions low and moderate UV index was registered mostly of winter period (June, July and August). Although it is evident very high UV index and extreme on the beginning of fall, on March and April, to be exactly and also in spring season (September, October and November).

Figure 4.7 – Frequency of maximum UV index per day, in percentage, from 2005 to 2017 presented according to the scale of colors of UV index, for all-sky condition (a) and clear-sky conditions (b).

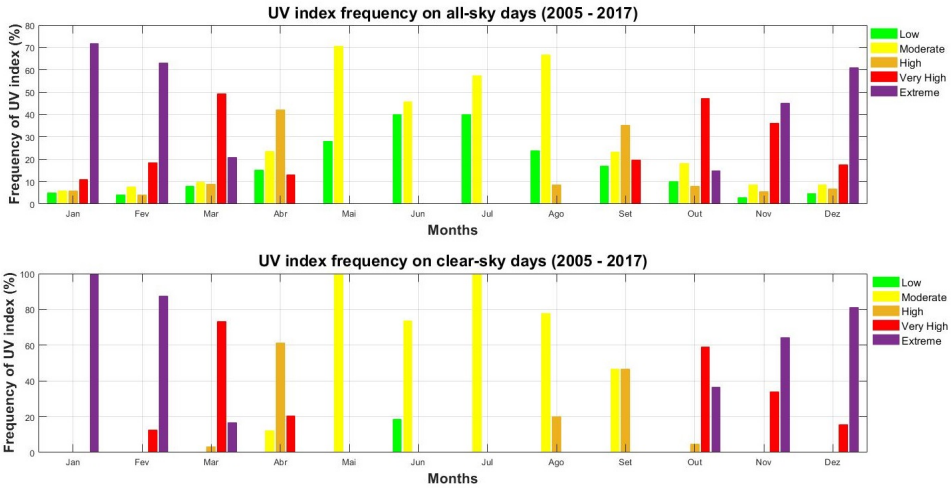

Source: Author.

During summer season the lowest percentage of extreme UV index was on December, in all-sky conditions extreme UV index was above 60% while in clear sky conditions was above 80% on the same month. Usually January is the hottest month in terms of temperature on the region. This month, extreme UV index occurred in more than 70% of days in all-sky conditions and 100% in clear sky condition. Similar behavior of UV radiation is observed in February, being more than 60 and more than 80%, respectively. It calls the attention in on clear-sky days, in October, very high UV index reaches 60% and almost all the 40% left was extreme UV index. A similar scenario happened in March, except very high UV index was almost 80%.

This is a very important analysis because evidences the influence of attenuation by clouds and also shows clearly that UV index reaches extreme and very high levels along the year, even in all-sky conditions, exactly when it is expected to have lower levels. September in all-sky conditions summed a total of 20% of days with very high UV index, differently from what was found for same month but with clear sky conditions. Cloud reflectivity of global irradiance (UV-A and UV-B) on the surface can be so significant at a point which levels are higher than in clear sky conditions. Effect that depends on the configuration, density and type of cloud coverage, according to Tiba & Leal (2017). So that it may be attributed to the increase of radiation due to cloud reflection.

On the other hand, depending on the same parameters cited before, UV radiation can be reduced until even 79% on the surface due to attenuation (GRANT; HEISLER, 2000; SCHAFER et al., 1996). Thus, days with clear sky condition end up resulting in higher UV index observed along the year, due to less attenuation by clouds. In this case, summer months resulted in more than 80% of days with extreme UV index. January stands out with

100% of the days with clear sky conditions, reaching its maximum UV index above extreme in the scale. Similar to what is seen in all-sky conditions days, except extreme UV index was between 60% and approximately 70% of the days, on summer season.

During summer season UV radiation tends to reach the highest levels of all year, although it was found in this study that mostly of the year UV radiation can reach critical levels. It is highly important to have those results in order to alert the population of the region and also create public awareness to avoid excess exposure. Many occupations require from employees to work outside, such as letter carrier. The region of study, the mail delivery is still done manually by workers that walk to mail destinations, construction workers are also frequently exposed, for example. Additionally, sunlight is crucial for human health due to synthesis of vitamin D. The results show that on the region of study solar radiation prevails mostly of the year alternating with rain and cloudy days providing enough sunlight to vitamin D synthesis.

4.2.2 Interannual variation of UV index

UV index data series used in the interannual variation study consists in a reconstruction of maximum UV index per day from Brewer, with all gaps filled with daily UV index measures from OMI/AURA. The maximum UV index per day, from Brewer measures, was selected from the clear-sky condition data set. It is usually from around mid-day measures. This series contains some gaps along the period, since the all-sky days are not included and also due to the periods when the equipment was out of operation. Each one of those days with missing data were filled with UV index collected from OMI. This data set is being refered as Brewer-OMI (Figure 4.8) and ranges from the year 2005 to 2017. Montlhy distribution of UV index Brewer-OMI data series (Figure 4.9) is consistent with seasonal behavior of UV radiation on the region. Climatology averages were obtained and applied in anomaly calculations in further study of wavelet analysis.

Figure 4.8 – Monthly UV index distribution Brewer-OMI measured around noon time, from 2005 to 2017.

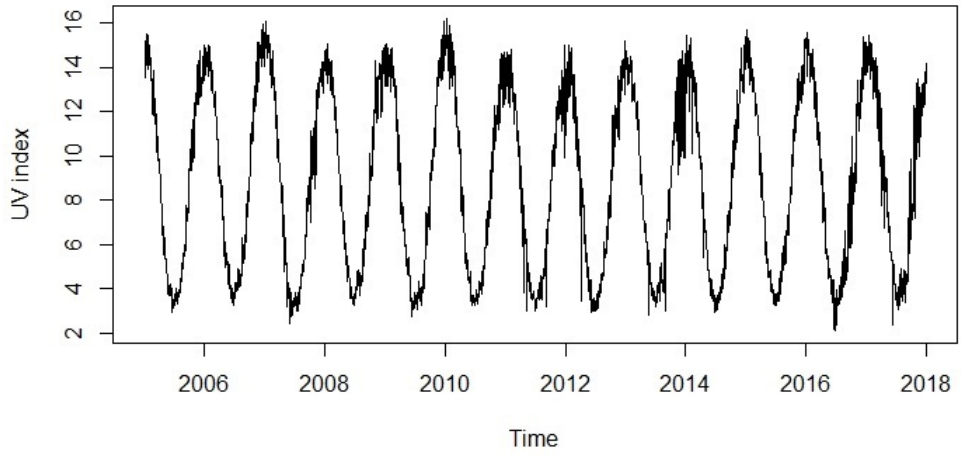

Source: Author.

Monthly climatology shows the seasonal pattern with lower variation in winter season than during summer and spring, as we see in error bars. On October a larger variation is observed, which might be linked to the period of events of secondary effects of Antarctic ozone hole. It is suggested further investigation regarding seasonal variations during this period of the year.

Figure 4.9 – Monthly climatology of UV index Brewer-OMI, from 2005 to 2017.

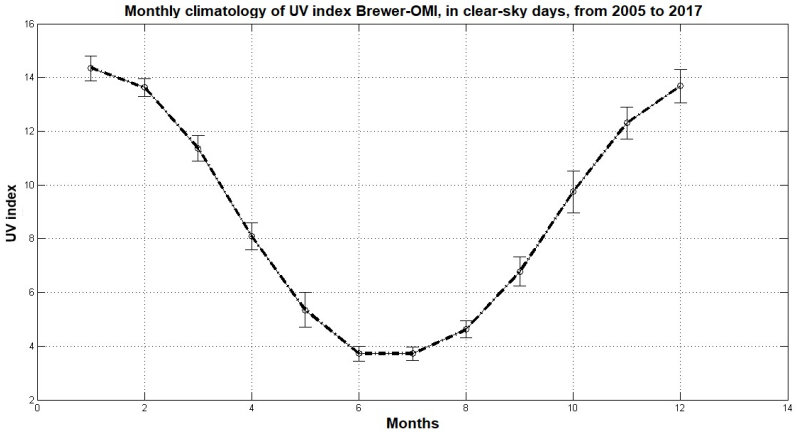

Source: Author.

Figure 4.10 contains the anomaly of Brewer-OMI data series in a), the wavelet power spectrum in b) showing in the region of 16 to 32 months the possible influence of QBO and in 64 months also the possible influence of ENSO. The region of 128 months it is seen the solar cycle influence, it is located outside the cone of influence due to the fact that the time series contains 12 years of data, while solar cycle is of approximate 11 years. Global wavelet spectrum in Figure 4.10 c) shows the same strong variations.

QBO and ENSO can cause variations to UV radiation, mainly due to the influence of those events in stratospheric ozone concentration and distribution in the atmosphere. It was found by Peres et al. (2017) through study using same ground instrument and in same location of this research, that QBO is the main responsible for inter-annual variability of ozone total column. Rigozo et al. (2012) had, previously, reported the influence of QBO on ozone. Also, through wavelet analysis, QBO signal was detected, indicating to be the possible reason of ozone seasonal variation on southern hemisphere.

Figure 4.10 – a) UV index anomaly of UV index data from Brewer-OMI, measured around noon time. b) wavelet power of UV index from Brewer-OMI and c) Global wavelet spectrum of UV index from Brewer-OMI.

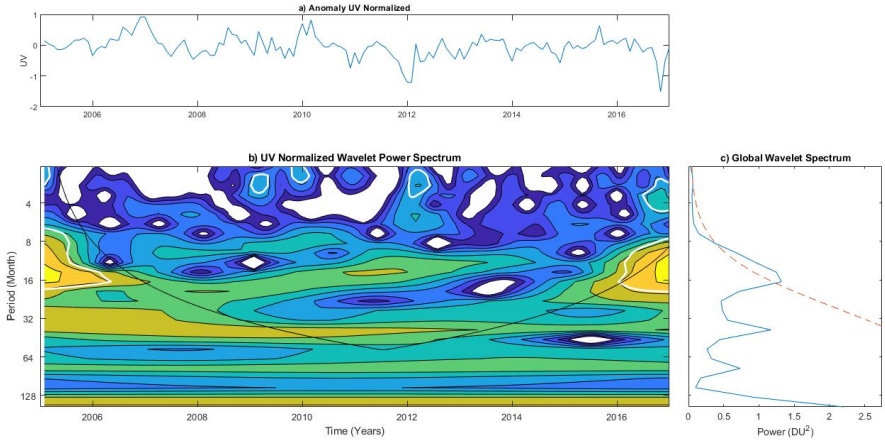

Source: Author.

Mid latitude regions were described by many authors as a highly ozone amplitude regions on account of the dynamic process that occur between meridian exchanges in stratosphere (PORTAFAIX et al., 2003). In this region the amplitude of ozone is controlled by seasonal cycles varying from approximately 260 Units Dobson in April and reaching its maximum in September, 295 Units Dobson (PERES et al., 2017).

Thereby, QBO effects in ozone on the region of study reflect in UV radiation as seen in wavelet analysis. East phase of QBO tends to increase UV irradiance while west phase of QBO decreases it, as evidenced by Troshichev & Gabis (1998). In addition, regarding to ozone, it tends to decrease in the second half phase of QBO due to an easterly shear that causes an upward circulation. The dynamic effects of QBO result in 5-year periodicity of UV-B radiation, which is more significant then variability caused by cloudiness (HERMAN et al., 2000).

Interference of El Niño phase of ENSO in stratospheric ozone is linked to its effect in the enhancement of up-welling Brewer-Dobson circulation in the tropical stratosphere, leading to a depletion in ozone in this region. While in La Niña phase the opposite happens, there is a weakening in the circulation, increasing ozone (MANATSA; MUKWADA, 2017). Changes in ozone total column due to ENSO effects result in erythemal UV changes on

clear sky condition of 6 to 10%, being El Niño the phase with greater effects on ozone total column (ZHANG et al., 2015).

Besides the influence of ENSO in ozone total column, it consists in a very important element in atmospheric inter-annual variability, changing the weather (KAYANO; ANDREOLI, 2006). Depending on the phase, it can intensify the rainfall in the region of study in case of El Niño meanwhile La Niña phase causes drought on the region. With intensity of rain on the region there is an increase in cloudiness and periods of droughts tend to result in more days with clear sky then interfering in UV radiation.

Regarding to influence of solar cycle in UV radiation, it can change even with short-term oscillations of solar activities, for example, solar flares can be responsible for the increase in UV radiation (TROSHICHEV; GABIS, 1998). Even if 11-year solar cycle is related to changes in intensity of UV-C at solar maximum, its impact in UV-B radiation was found to be not so significant, less than 1% (KERR; FIOLETOV, 2008). The major impact of solar activity on UV-B is actually due to its interference in stratospheric ozone production. With enhancement of solar activity there is increase of ozone production which leads to a major absorption of UV radiation therefore more attenuation of UV-B radiation on the surface (ROZEMA et al., 2002).

It is important to determine interannual variations to know what other oscillations interfere in surface UV at the study region and also to know how and with what frequency. Here it is seen the effects on surface UV by QBO and ENSO, attributed to their strong influence in concentration and distribution of stratospheric ozone. Solar cycle also is accounted as an important factor for UV radiation intensity even though on the time series analyzed in the present study was of twelve years. It is recommended to extend the time series in future studies to have a wider perspective of solar cycle influence on surface UV radiation on the region. As it is also recommended the investigation of aerosol influence on UV index levels.

4.2.3 Seasonal variation of Erythema dose

Erythema distribution, seen in Figure 4.11, plot a, from 2005 to 2017. It shows a maximum dose of 400 mW/m^2, which is much higher than the minimum dose to cause damage in photo-types I and II and very proximate of the minimum dose to affect photo-types III and IV (FITZPATRICK, 1988). Observing the daily (plot b) and monthly mean (plot c) of Erythema dose for the same period, doses are relatively low but still can affect photo-types I and II.

Erythema dose was observed separately in each season (Figure 4.12) and for all-sky conditions it shows a concerning daily mean only on summer (a). However maximum doses along the year indicate that photo-types I and II are exposed to its maximum dose at

Figure 4.11 – Daily data distribution Erythema dose (mW/m^2) on all-sky condition, 2005 to 2017 (a). Erythema dose distribution with all measures of UV index (blue dots), in all-sky conditions, from 2005 to 2017. Daily mean of Erythema dose (b), in yellow line, shows the mean of all measures in all-sky conditions of Erythema dose per hour of day. Standard deviation in dashed lines, and the maximum Erythema dose registered per hour of day are represented in purple diamonds. Monthly climatology of all measures in all-sky conditions are distributed along the months of the year per hour of day (c), the plot was adapted for better visualization of UV index which is represented in color bar.

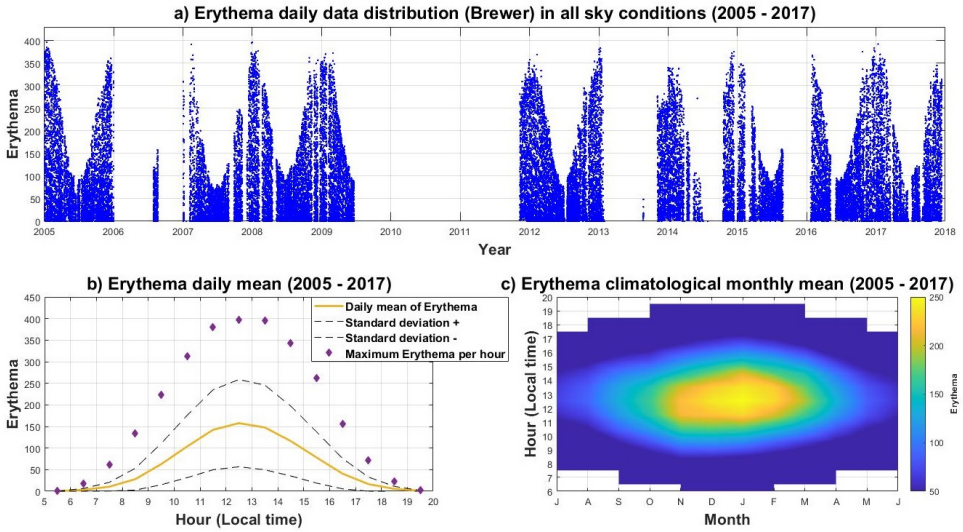

Source: Author.

least three seasons of the year.

Erythema dose on clear sky days are distributed along the period of study, on Figure 4.13 plot on top, the plot below on the left shows the distribution of maximum erythema dose per hour. Monthly mean is seen in Figure 34 plot below on the right, shows a dose of approximately 400 mW/m^2 at least along 4 months of the years, being from mid-October to December and continuing the following year from January to early March. Predominantly, from March to April and then between September and October erythema dose remains between 300 and 350 mW/m^2. It shows certain concern for all skin types. Months of April and May, as well as, August to early September, indicate that skin type I can be exposed to maximum erythema dose, since it indicates a mean of 250 mW/m^2.

Figure 4.12 – Daily mean of Erythema dose (mW/m^2) on all-sky condition (yellow line) per season, summer (a),autumn (b), winter (c) and spring (d). Standard deviation is the dashed line and maximum Erythema dose per hour of day is indicated with purple diamonds. The daily means are from all measures in all-sky conditions from 2005 to 2017.

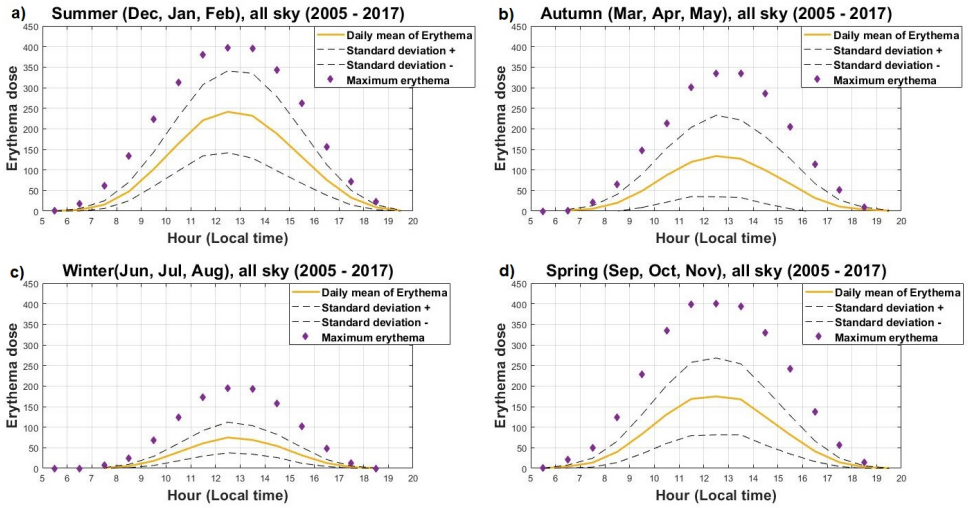

Source: Author.

Figure 4.13 – Daily data distribution of Erythema dose (mW/m^2)on clear-sky condition, 2005 to 2017. Erythema dose distribution with all measures of UV index (blue dots), in clear-sky conditions, from 2005 to 2017. Daily mean of Erythema dose, in yellow line, shows the mean of all measures in clear-sky conditions of Erythema dose per hour of day. Standard deviation in dashed lines, and the maximum Erythema dose registered per hour of day are represented in purple diamonds. Monthly climatology of all measures in clear-sky conditions are distributed along the months of the year per hour of day, the plot was adapted for better visualization of UV index which is represented in color bar.

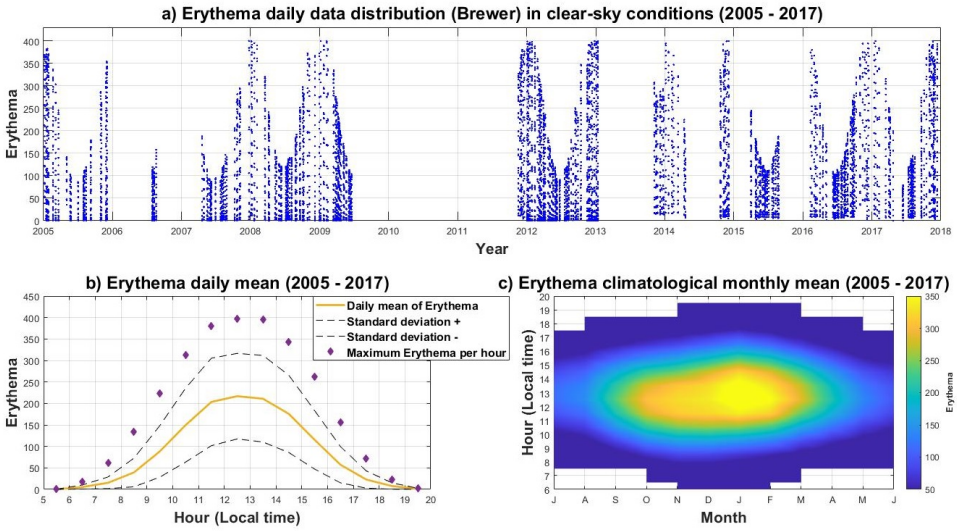

Source: Author.

Diurnal mean of Erythema shows relatively low values, being the mean close to 200 mW/m^2 between 12 and 13 hours, with a standard deviation from 100 to 300, although

maximum doses per day were registered around 400 mW/m^2. When observing erythema dose closely by season, it corroborates with results found in monthly mean. Summer season (Figure 4.14) present a maximum daily mean dose of almost 350 mW/m^2. Naturally, it reduces during autumn and reaches its minimum during winter, ranging the daily mean between a dose of 200 and a 100 mW/m^2 along this period. However, the maximum registered in those seasons were almost 350 and 200 mW/m^2, respectively. Erythema dose rises during spring, with a daily mean of more than 250 mW/m^2, with a maximum dose of 400 mW/m^2. This analysis shows that at least 6 months of the year, erythema doses can affect skin types I to IV.

Figure 4.14 – Daily mean of Erythema dose (mW/m^2) on clear-sky condition (yellow line) per season, summer (a), autumn (b), winter (c) and spring (d). Standard deviation is the dashed line and maximum Erythema dose per hour of day is indicated with purple diamonds. The daily means are from all measures in clear-sky conditions from 2005 to 2017.

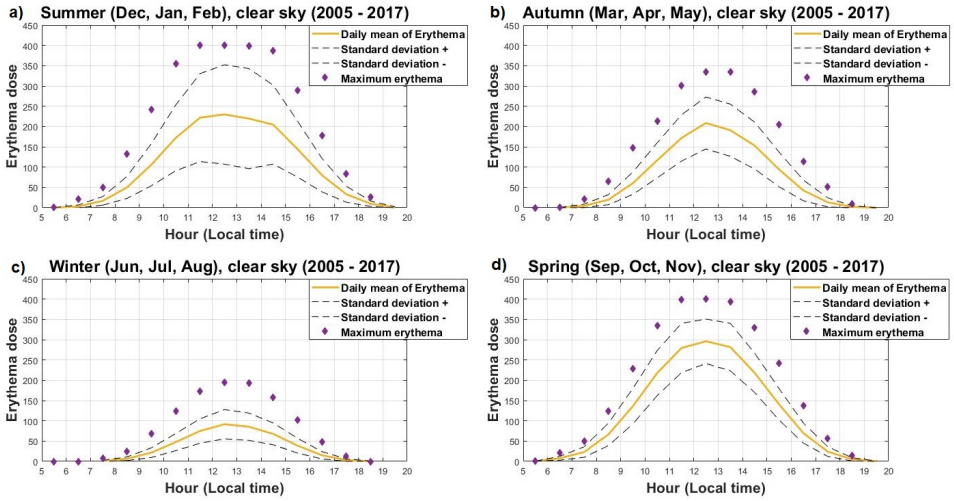

Source: Author.

A study conducted by Corrêa & Pires (2013) on the evaluation of UV radiation measures in Brazil, showed that the whole Brazilian country receive high levels of UV radiation, being the region of São Paulo with the maximum daily doses, reaching 24 times the minimum erythema dose for phototype II. And yet on winter season it is still high in many regions of the country, when erythema daily dose reached more than twenty times the maximum recommended by World Health Organization. What reassure the importance of research in this area and to study the intensity of UV radiation in the south region of Brazil.

An estimation of cases of skin cancer, type melanoma, on the region of study points to 290 cases among men and 280 cases among women, in 2020. Which is higher than the estimation in Rio de Janeiro state, for example where is closer from the tropics and famous for the beach life. The estimation for skin cancer non melanoma in Rio Grande do Sul was 8.850 and 6.650 between men and women, respectively (SILVA, 2019).

The region of study has a European history of colonization, being the state divided

in four cultural regions due to its ethnic presence. Besides natives, Portuguese, Spanish, African, Azorean, Germanic and Italian were also part of colonization of the region. Mostly of the decedents of this land carry the characteristics of white skin, corresponding to phototype groups I to IV. According to IBGE (2013), 82.4% of the population of the state of Rio Grande do Sul is white. Which arises the concern for skin protection measures when sun exposed at certain periods of the day and the year.

Anomaly and wavelet analysis indicated interannual variations can be influenced by other circulations. Influences of solar cycle, ENSO and QBO are seen in UV radiation intensity on the region. Since QBO affects ozone distribution on the stratosphere, it is observed more intensity in UV radiation. Also, ENSO influenced increasing cloudiness and lowering down UV radiation intensity. 11-years solar cycle is present along all the period since data range is of 12 years.

4.3 ULTRAVIOLET RADIATION AND EFFECTIVE OZONE

Daily integral of UV radiation measured with Brewer is used in the calculation of Erytema dose and UV index. It was compared with effective ozone, between 2005 and 2017. Effective ozone is obtained from ozone total column considering the solar zenith angle at the time of ozone measurement.

Distribution of UV daily integral and effective ozone data along the period (Figure 4.15 a), show evidence of the increase response of UV when concentration of ozone lows down. The same is observed in the correlation, showing high correlation between them, with a correlation coefficient (R) of -0.84 (Figure 4.15 b). Confirming the elevation in UV when there is a drop in ozone total column.

The use of this method for estimating effective ozone has been validated by Bertagnolli et al. (2005), in south of Brazil and Nozawa et al. (2007) in Japan, Brazil and Chile, where in both studies found results of an exponential with anti-correlation and coefficient close to found in this study, between UV radiation and effective ozone.

Figure 4.15 – Time series of the UV daily integral (J/m^2) and effective ozone (Dobson Units) from 2005 to 2017 (a) and correlation between both series (b).

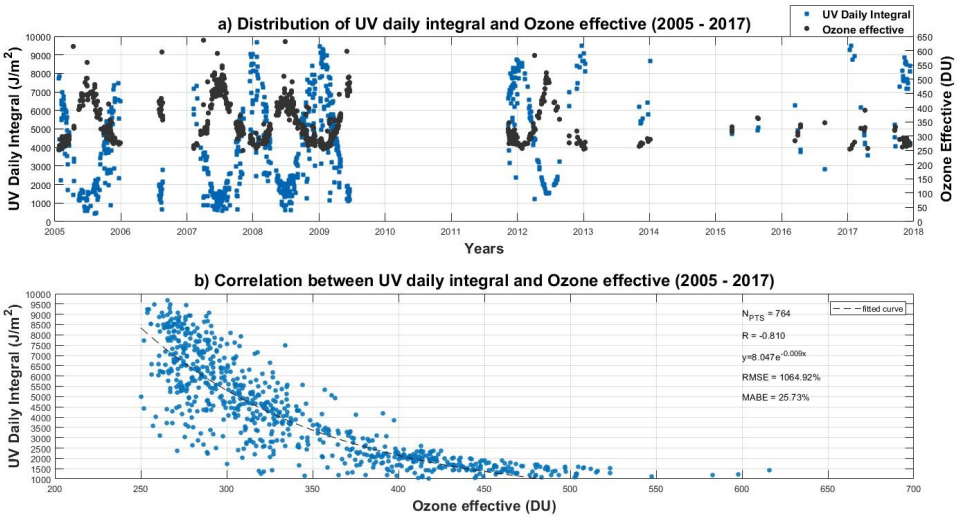

Source: Author.

4.4 UV RADIATION BEHAVIOR ON EVENTS OF SECONDARY EFFECTS OF OZONE HOLE

Many events were identified between 2005 and 2016 (BITTENCOURT et al., 2018b) in the same region of this study, ten events were selected to be studied here and one of those events was thoroughly described in this research. The events were selected based on the availability of ground data of UV index and UV-B, considering there are many gaps in the UV radiation data series. Other important consideration in the selection of events was the sky condition.

It is very complex to determine the exactly amount of UV radiation incident on the surface when in presence of clouds, as well as to precise the time when UV radiation is more or less intense with a cloudy sky. Since in cloudy days the resulting effects of variation of ozone total column on UV radiation could be masked and lead us to erroneous results (GUARNIERI et al., 2004), then it was considered in the analysis of the events of secondary effects of Antarctic ozone hole, only days with clear-sky conditions.

It is important to emphasize the persistence of ozone poor air masses over the region of study for a couple of days until ozone total column is reestablished (BITTENCOURT et al., 2018a). Based on that, it was defined one clear sky-day during the days of events to be looked closely. Ozone total column of this day was compared with UV index (Table 4.1) and UV-B non-weighted (Table 4.2), separately. The daily values were compared with monthly climatological average, used as a reference here to evaluate how much depletion of ozone

and increase of UV radiation there were. So that, the percentage of increase of UV index and UV-B non-weighted was calculated as well as the percentage decrease of ozone total column.

Among all events studied in this research regarding to UV index and ozone total column analysis (Table 4.1), 60% resulted in 4% UV index increase for each 1% ozone total column depletion, with the exception of the one on October 14, 2012 which resulted in 3.65% increase in UV index, even though a very high increase. Two events showed increase of UV index higher than 4% while only 1 event had an increase of 1% of UV index for a 1% depletion of ozone total column.

Ozone total column ranged between 220 and 260 DU around the days of events. It was observed that ozone total column tends to decrease rapidly on the events, furthermore it takes a few days to be reestablished, tending to increase slowly and gradually. Thus, the polar air masses poor in ozone arrive on the region of study and they can be persistent over the location for a few days, being observed that it takes a mean of two days to ozone total column start to be reestablished and almost 5 days to ozone total column reach the monthly climatological average after the first day of event. Those effects on ozone total column reflect on surface UV.

There were two events accounted in 2005, the one in September shows an increase of UV index of almost 1% more than the event in October. That could be related to different climatological mean of each month that varies from 6.01 in September to 7.96 in October, even though the ozone total column decrease in the event of September was 2.8% higher than in October. Only one event was accounted in 2007, it occurred in October and despite of the 8% ozone total column depletion there was an increase in UV index of 8%, in regard to the climatological mean. There was the slightly increase of 1% of UV index for each 1% ozone total column decrease.

The two events occurred in 2008 are similar to the ones from 2005 except they appeared to be more intense, specially the one in September, as in terms of decrease in ozone total column as in terms of the increase of UV index. Even though the climatological mean is lower in September, the ozone depletion was very significant, leading to almost 59% UV index increase. The event on October, 2008 ozone depletion was only 2,6% less than the previous event however resulted in 81% increase in UV index, leading to extreme UV index and resulting in the alarming 6,7% UV index increase for each 1% ozone depletion.

In 2012 there were three events included here. Two events in September with a very similar behavior, with almost 10% ozone depletion but with the significant increase of 40% of UV index in the first and the second only 6,6% ozone decrease which resulted in 34% UV index increase, both of them UV index reached very high, according to the scale. One event in October, 2012 showed different behavior, UV index reached extreme and ozone depletion was more significant than the previous ones, 13% lower than the climatological mean.

Table 4.1 – Events of secondary effects of AOH in clear sky condition considering the UV index of the day and climatological mean of UV index of the month.

Date	UV index	Climatological mean UV index	Increase of UV index (%)	Ozone total column (DU)	Climatological mean Ozone (DU)	Decrease of Ozone (%)	Increase of UV index with 1% O_3 decrease (%)
29/09/2005	9.43	6.01	56.9	261.95	296.97	-11.8	4.8
11/10/2005	10.88	7.96	36.7	264.76	290.79	-9.0	4.1
08/10/2007	8.65	7.96	8.7	267.58	290.79	-8.0	1.1
28/09/2008	9.55	6.01	58.9	253.12	296.97	-14.8	4.0
27/10/2008	14.45	7.96	81.5	255.32	290.79	-12.2	6.7
14/09/2012	8.44	6.01	40.4	267.79	296.97	-9.8	4.1
22/09/2012	8.09	6.01	34.6	277.41	296.97	-6.6	5.3
14/10/2012	11.78	7.96	48.0	252.67	290.79	-13.1	3.7
25/08/2016	6.15	3.98	54.5	252.85	290.06	-12.8	4.3
21/10/2016	15.02	7.96	88.7	233.29	290.79	-19.8	4.5

Table 4.2 – Events of secondary effects of AOH in clear sky condition considering the UV-B non-weighted (W/m^2)$of the day and climatological mean of UV-B non-weighted of the month.$

Date	UV-B (W/m^2)	Climatological mean UV-B (W/m^2)	Increase of UV-B (W/m^2)(%)	Ozone total column (DU)	Climatological mean Ozone (DU)	Decrease of Ozone (%)	Increase of UV-B with 1% O_3 decrease (%)
29/09/2005	1669	638	161.7	261.95	296.97	-11.8	13.7
11/10/2005	1885	764	146.7	264.76	290.79	-9.0	16.4
08/10/2007	1354	764	77.2	267.58	290.79	-8.0	9.7
28/09/2008	1655	638	159.4	253.12	296.97	-14.8	10.8
27/10/2008	2480	764	224.6	255.32	290.79	-12.2	18.4
14/09/2012	1366	638	114.1	267.79	296.97	-9.8	11.6
22/09/2012	1303	638	104.2	277.41	296.97	-6.6	15.8
14/10/2012	1886	764	146.9	252.67	290.79	-13.1	11.2
25/08/2016	1112	417	166.7	252.85	290.06	-12.8	13.0
21/10/2016	2348	764	207.3	233.29	290.79	19.8	10.5

Two events occurred in 2016 were selected. One event in August resulted in more than 50% increase in UV index due to a 12,8% ozone content depletion. Meaning a 4,3% increase in UV index for each 1% ozone decrease. Although the event was significant in terms of increase of UV radiation, UV index reached high in the scale, probably due to the winter season, when UV radiation is naturally lower. The second event from 2016 was considered a major event of ozone depletion and as a consequence UV radiation increase. Thus this event was chosen as a study case in the following session.

UV-B non-weighted is a measure of UV-B without any filters such as biological filters of DNA, erythema or UV index, so that it is important to be compared with ozone total column. Differently from UV index analysis, the analysis of UV-B non-weighted, in Table 4.2, showed a very significant increase with ozone depletion, which is expected since it is a direct measured.

The exact same ten events from previous analysis with UV index were studied using UV-B non-weighted measures. The events in 2005 were very similar, with greater increase of UV index in the event of September but almost extreme UV index reached in the event of October. The event in 2007 had minor effects on UV index compared with all the other events, resulting in only 9.1% UV index increase for each 1% ozone depletion. UV index that day was slightly above climatological mean. There were two events in 2008, being the one occurred in October with the major increase of UV index. It was 224% higher then the climatological mean, resulting in UV-B non-weighted of 2480 W/m^2.

All three events occurred in 2012 were very similar regarding to the increase of UV-B non-weighted. A curious detail in the event on September 22 when the decrease in ozone total column was of 6% in relation to the climatological mean and the increase of UV-B non-weighted was 15% for each 1% ozone depletion, while the other event, in September 14 the drop was 9%, leading to 11% UV-B increase for each 1% ozone depletion. This could be due to the second event is in the end of September is closer to October when the UV radiation naturally intensifies, due to the change of seasons. In addition, the event in October 14, showed same behavior of the first event in September, probably due to the higher climatological mean. The three events had an increase of more then 100% in UV-B non-weighted.

In 2016 there was one event in August, with more than 150% increase in UV-B non-weighted, it resulted in 13% increase in UV-B for each 1% ozone depletion. The increase of UV-B non-weighted in the event of October 21, 2016 was more than 200% with 19% ozone content depletion. Generally, the daily values of UV-B on the days of events selected are at least 100% higher than the climatological monthly mean, with only one exception. Daily values reached more than 200% increase in two events, Ocotober 27, 2008 and August 25, 2016. The event on October, 2007 showed the lowest increase of UV-B, resulted in 77% of increase in relation with the climatological mean. Overall, the mean of UV-B non-weighted increase with 1% decrease of ozone total column was 13%.

A study developed by Guarnieri et al. (2004) on the same location of the present study, showed a major influence of ozone variation on UV-B radiation, suggesting 94% of UV radiation variability would have been caused by ozone changes when analyzing clear sky days. Resulting in a UV-B enhancement ranging from 0.87% to 1.43%, depending on the solar zenith angle, for each 1% of ozone depletion. Regarding to ozone total column, a usual content on the region of study consists in approximate 280 DU which is also observed on the months studied, usually far from the day of event. Concentrations that are characteristic of the ozone hole are values below 220 DU, on the Antarctic region (HOFMANN et al., 1997).

Preez et al. (2019) estimated in his study in South Africa, in clear-sky conditions 1% decrease of ozone total column would result in 0.59% increase of UVB radiation on the surface, using clear-sky determination method of radiation amplification factor. In the same study, specifically, in events of ozone depletion and with clear-sky conditions, UV radiation increases from 6 to 45% with variations in ozone total column. Reported by Raptis et al. (2021) as a rare low ozone event, in the region of Athens, Greece, caused the increase of approximately 30% in the UV radiation, when the decrease in ozone total column was of 15% in relation to the climatological monthly mean.

Generally, the decrease in ozone total column with the arrival of polar masses appear to be more intense in the year of 2008 and from 2012 until 2016, despite the positive scenario describing the healing of Antarctic ozone hole by Solomon et al. (2016). The response of UV index to lower ozone content, is in similar proportion, with few exceptions. The events on September appear to be have major ozone decrease than the events in October, probably because it is the first period of weakening of Polar vortex, releasing filaments with lowest ozone content. With exception of event of October, 2016, probably due to the time of year when radiation already tends to be higher.

Through this research it was filled a gap regarding updates in UV radiation and events of secondary effects of Antarctic ozone hole specific on the south region Brazil. It is suggested the investigation of more events in future studies. Aside of that, different mid-latitude regions could be studied regarding UV radiation behavior during those events, besides south of Brazil. Since aerosol loads can interfere on UV radiation intensity on the surface, those measurements from Brewer spectrophotometer could also be accounted for future studies of UV radiation on the region.

4.5 STUDY CASE: EVENT OF OCTOBER, 2016

The study case is about one of the most significant event of secondary effects of Antarctic ozone hole, occurred between 2005 and 2016 and considered one of the most intense event in the last 25 years. This event was persistent starting from October 20, 2016

and it is detailed discussed in this section. Ozone total column measured with the Brewer spectrophotometer used in this study, was 225.5 Dobson Units on October 20, there was a 23% decrease in relation to the climatological mean for October (from 1992 to 2016), a very critical reduction as reported by Bittencourt et al. (2018a). The following day, October 21, the poor-ozone air mass was still on the region but showed a slightly recover, ozone total column was 19% below the climatological mean. With the observation of extreme reduction in ozone total column in relation to the climatological mean, it was identified the event.

Then, The potential vorticity analysis confirmed the origin of air mass is from Antarctic region. It acts as a dynamic tracer for those large air-masses and is correlated with the transport of chemical constituents traces, as ozone. Figure 4.16 shows the maps of potential vorticity in the level of potential temperature of 700 Kelvin. It is observed its progress towards the study region. The images show the increase in Absolute potential vorticity, indicating the reduction in ozone content.

Figure 4.16 – Potential vorticity at potential temperature level of 700 K, on October 19 (a), 20 (b), 21 (c) and 22 (d) 2016 at the region of study (highlighted in a, b and c. The scale of colors varies from 0 to 260.

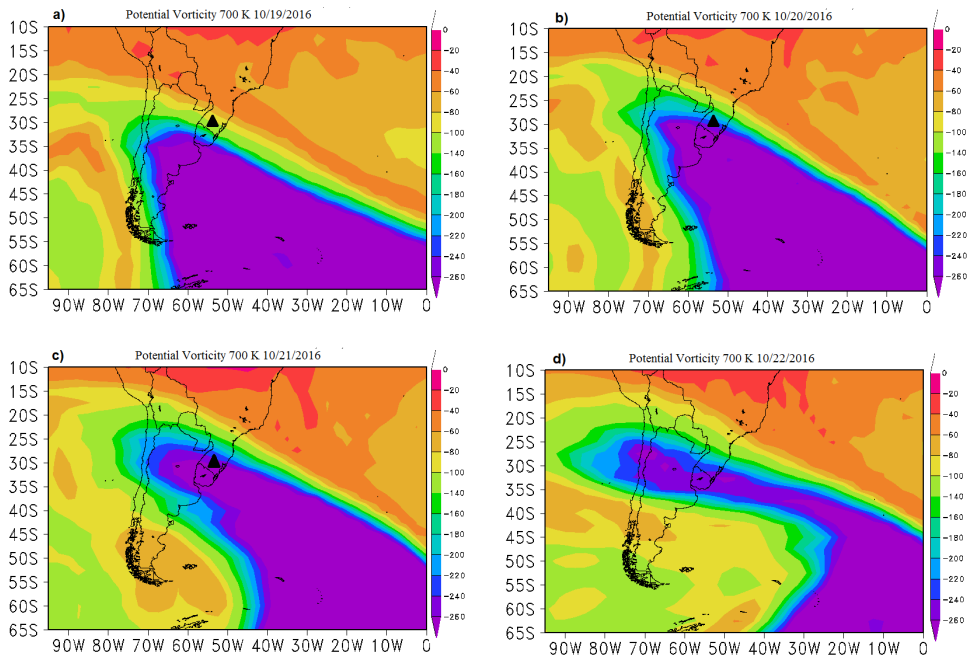

Source: (BITTENCOURT et al., 2018a)

Images of October 19 to 21, 2016 from OMI satellite (Figure (4.17) in a global and South Pole perspectives show AOH over the region and its influence in mid-latitude regions. According to these images, poor-ozone air masses that reached the region of study range from 250 and 200 Dobson Units, while in South Pole region ozone content is even lower.

The study of the backward trajectories of ozone-poor air masses in different heights are shown in Figure (4.18). It is an image from HYSPLIT, a model from NOAA that shows

Figure 4.17 – Image of OMI satellite showing ozone total column (Dobson Units) depletion on Antarctic region and its influence over south of Brazil.

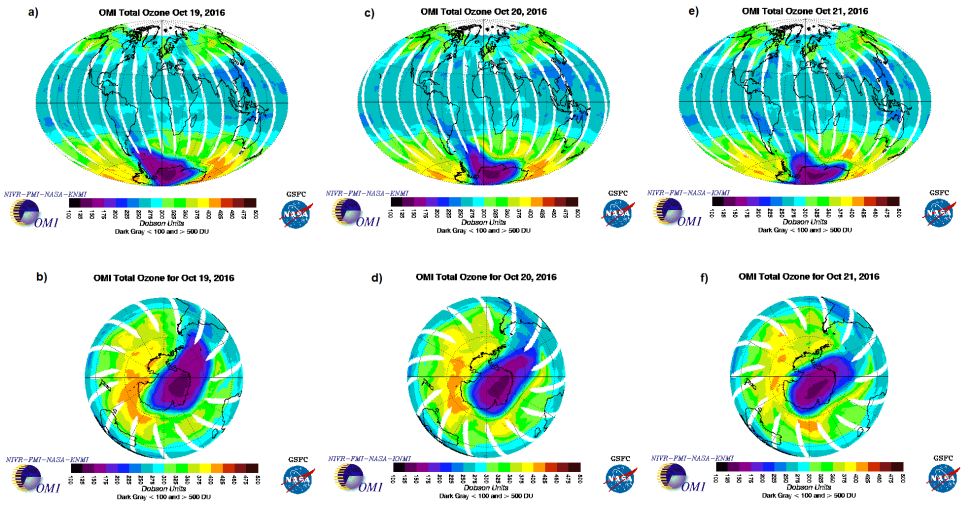

Source: (BITTENCOURT et al., 2018a)

the air mass dispersion and it is used to trace air mass trajectories. It contains the path followed by ozone-poor air masses in October 20 (a) and 21 (b), 2016, at 28, 24 and 20 km height and it is seen it reached the study region (BRESCIANI et al., 2018).

The day selected to have UV radiation analyzed was October 21 due to the clear-sky condition, confirmed using the method previously described of Gaussian analysis. Maximum UV index per day between October 10 and 31, 2016 is shown in Figure 4.19, as well as daily ozone total column. An image via GOES 13 Satellite of thermal infrared channel shows the absence of clouds at this day (Figure 4.20).

UV index was 10 (very high in UV index scale), on October 20, however, on the day after, October 21, UV index from Brewer reached 15 while the climatological monthly mean is almost 8 in UV index scale. It resulted in 88.53% increase in UV index in relation to the climatological mean of the month, while the anomaly of ozone total column was -19.77% in relation to the climatological mean of the month. The following days, UV index levels slowly diminished as ozone total column gradually recovered.

This was considered the most significant day in UV radiation increase, each 1% reduction in ozone total column there was an increase of 4.47% in UV index. Apparently, air mass poor in ozone was persistent for five days. It was suggested by Bittencourt et al. (2018a) the air transport between stratosphere and troposphere were intensified by the presence of subtropical jet combined with positive omega values at 500 hPa, which might be one of the responsible factors for such extreme event.

The identification of numerous events of secondary effects of Antarctic ozone hole enabled to learn UV radiation response on the south of Brazil. It was confirmed the fast response of UV radiation in reduction of ozone total column and the alarming levels reached by UV index during the events. It is crucial information for public health because once the

Figure 4.18 – Backward trajectories of HYSPLIT/NOAA model, of poor-ozone air mass reaching the south of Brazil in three different heights 28 km (green), 24 km (blue) and 20 km (red), on October 20 (a) and 21 (b), 2016 .

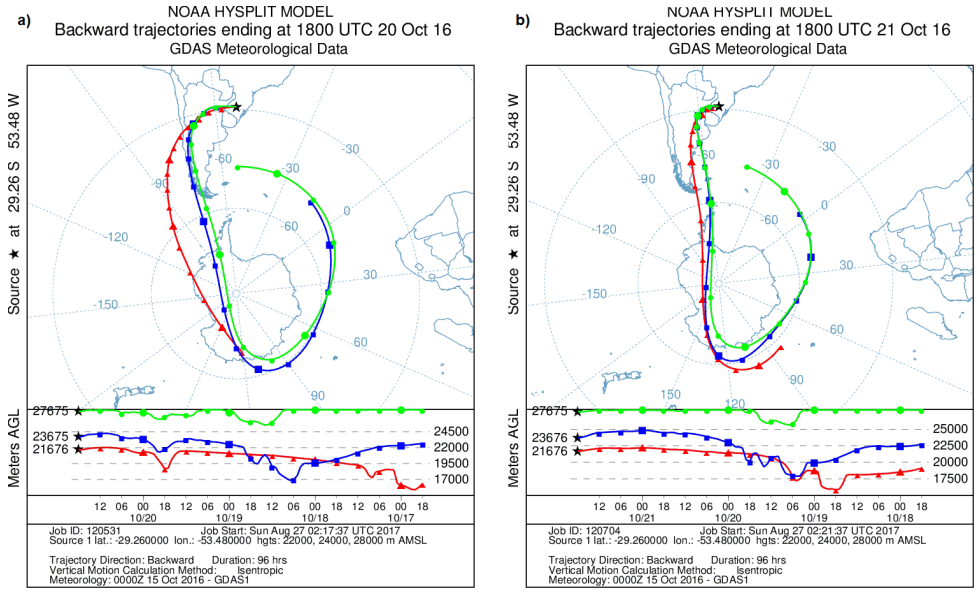

Source: (BITTENCOURT et al., 2018a)

population is aware about the existence and how these events impact surface solar UV, precautions can be taken. Besides human health, the increase in UV radiation during this period also affects fauna and flora, another concern to be considered when finding ways to mitigate the effects of the events of secondary effects of AOH.

Besides health issues related to excess exposure to UV radiation, sunlight is essential to human life in many ways. The synthesis of vitamin D only happens with skin exposure to the sun and it is known that this hormone plays a key role in immune system of the body. Aranow (2011) said "Vitamin D can modulate the innate and adaptive immune responses. Deficiency in vitamin D is associated with increase autoimmunity and an increased susceptibility to infection". Vitamin D is directly linked to the promotion of bone health because it enhances calcium absorption besides the mineralization of the collagen matrix in bone. In such manner, population is provided with a great amount of solar radiation enabling the syntheses of vitamin D through sunbath. Results founded in this study are extremely important and could be used for a public campaign with accessible information about this matter to rise public awareness about occurrence period, region of impact and how it affects human and animal health.

Figure 4.19 – UV index (red doted-line) from Brewer and Ozone total column (Dobson Units) (blue doted-line) from Brewer and OMI, in October, 21 2016 (black circle).

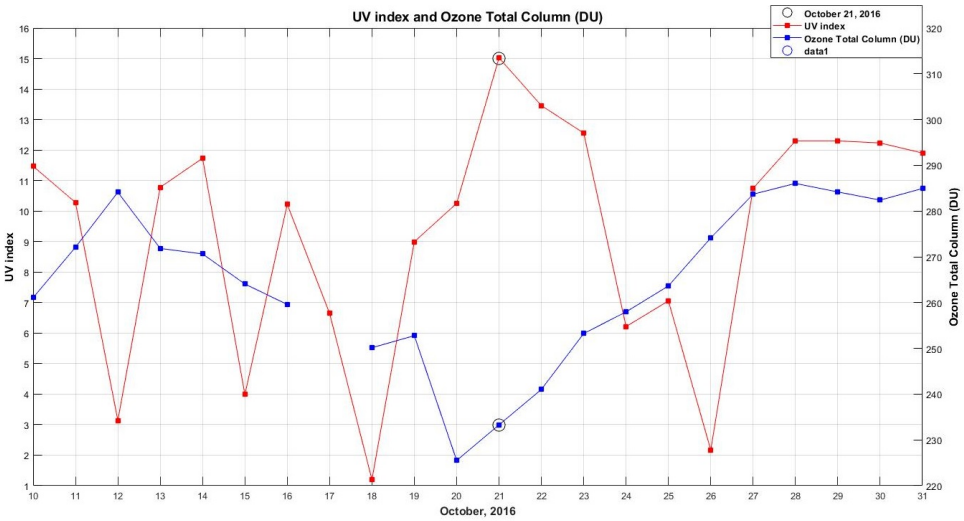

Source: Author.

Figure 4.20 – Satellite image GOES 13, infrared thermal channel at 15 hours, local time, on October, 20 2016.

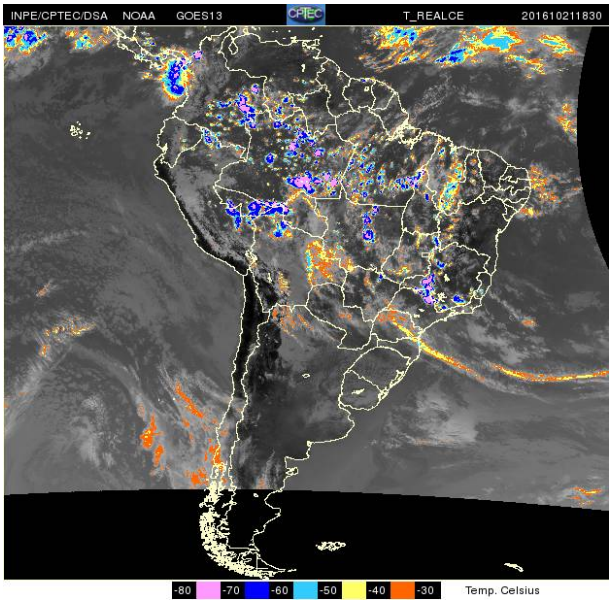

Source: CPTEC/INPE, 2017.

5 CONCLUSIONS

A total of 12 years, from 2005 to 2017, of measurements of UV index collected with a Brewer Spectrophotometer (MKIII #167), in the south region of Brazil, were carefully analyzed to determine the variation of UV index in the region, considering cloud cover attenuation, circulations influencing and most important, the behavior of UV index in events of secondary effects of Antarctic ozone hole.

Maximum daily measures of UV index data from ground instrument was compared to satellite-derived UV index levels available from OMI/AURA. They have the same pattern and the comparison resulted in a correlation coefficient of 0.95.

Cloud fraction and images from an All Sky camera supported the selection of days with clear-sky conditions with observation of irradiance curve. Considering the effects of clouds on UV index, it was evident the cloud attenuation since the daily mean of UV index on clear-sky days, from 2005 to 2017, increased 33% when comparing with all-sky condition.

Looking at each season, daily means of all seasons showed that high levels of UV index occur at least in 20% of seven months of the year in clear sky conditions. The study of the frequency of UV index in clear-sky days, showed during six months of the year there are extreme and very high UV index. Extreme UV index vary between 100% and almost 20% among summer, spring and autumn season.

Erythema dose analysis considered maximum doses for each phototype as a reference. During six months of the years all four skin types can be affected by the doses measured. Taking into account that mostly of population in study region have skin type more susceptible to solar damage, it is important to arise this matter in the community.

The first study regarding UV radiation and ozone total column conducted was the UV daily integral compared with ozone effective. It showed the quick response of UV radiation with decrease in ozone total column.

A total of 10 events were selected to be studied, one of them were thoroughly discussed. All events show a very significant UV radiation increase. UV index was extreme and very high in 90% of the events, the percentage increase in UV index was from 8.7% to 88.7%, being this the most critical one, in October, 2016. Considering all events, the average increase in UV index was 4% for each 1% ozone total column depletion.

Average increase of UV-B non-weighted is in larger scale than UV index because of type of UV radiation measure, without biological filters. It resulted in 13% increase of UV-B non-weighted for each 1% ozone total column depletion. Showing how intense surface UV radiation can become during events of secondary effects of Antarctic ozone hole.

BIBLIOGRAPHY

ANTÓN, M. et al. Total ozone mapping spectrometer retrievals of noon erythemal-cie ultraviolet irradiance compared with brewer ground-based measurements at el arenosillo (southwestern spain). **Journal of Geophysical Research: Atmospheres**, Wiley Online Library, v. 112, n. D11, 2007.

____. Comparison of uv irradiances from aura/ozone monitoring instrument (omi) with brewer measurements at el arenosillo (spain)–part 1: Analysis of parameter influence. **Atmospheric Chemistry and Physics**, Copernicus GmbH, v. 10, n. 13, p. 5979–5989, 2010.

ARANOW, C. Vitamin d and the immune system. **Journal of investigative medicine**, BMJ Publishing Group Limited, v. 59, n. 6, p. 881–886, 2011.

ARTAXO, P. et al. Efeitos climáticos de partículas de aerossóis biogênicos e emitidos em queimadas na amazônia. **Revista brasileira de meteorologia**, v. 21, n. 3a, p. 168–22, 2006.

BAE, M.; KIM, H. The role of vitamin c, vitamin d, and selenium in immune system against covid-19. **Molecules**, Multidisciplinary Digital Publishing Institute, v. 25, n. 22, p. 5346, 2020.

BERTAGNOLLI, C. et al. Modelo para cálculo da coluna total de ozônio usando dados do espectroradiômetro do observatório espacial do sul. In: EUROPEAN ASSOCIATION OF GEOSCIENTISTS & ENGINEERS. **9th International Congress of the Brazilian Geophysical Society**. [S.l.], 2005. p. cp–160.

BITTENCOURT, G. D. et al. A major event of antarctic ozone hole influence in southern brazil in october 2016: an analysis of tropospheric and stratospheric dynamics. In: COPERNICUS GMBH. **Annales Geophysicae**. [S.l.], 2018. v. 36, n. 2, p. 415–424.

____. Influência da dinâmica atmosférica durante eventos de efeito secundário do buraco de ozônio antártico sobre o sul do brasil. Universidade Federal de Santa Maria, 2018.

BOWMAN, K. P. Global patterns of the quasi-biennial oscillation in total ozone. **Journal of atmospheric Sciences**, v. 46, n. 21, p. 3328–3343, 1989.

BRESCIANI, C. et al. Report of a large depletion in the ozone layer over southern brazil and uruguay by using multi-instrumental data. In: COPERNICUS GMBH. **Annales Geophysicae**. [S.l.], 2018. v. 36, n. 2, p. 405–413.

BREWER, A. Evidence for a world circulation provided by the measurements of helium and water vapour distribution in the stratosphere. **Quarterly Journal of the Royal Meteorological Society**, Wiley Online Library, v. 75, n. 326, p. 351–363, 1949.

BUNGE, C.-A.; BECKERS, M.; GRIES, T. **Polymer Optical Fibres: Fibre Types, Materials, Fabrication, Characterisation and Applications**. [S.l.]: Woodhead Publishing, 2016.

CADET, J.; SAGE, E.; DOUKI, T. Ultraviolet radiation-mediated damage to cellular dna. **Mutation Research/Fundamental and Molecular Mechanisms of Mutagenesis**, Elsevier, v. 571, n. 1-2, p. 3–17, 2005.

CADET, J.-M. et al. Comparison of ground-based and satellite-derived solar uv index levels at six south african sites. **International journal of environmental research and public health**, Multidisciplinary Digital Publishing Institute, v. 14, n. 11, p. 1384, 2017.

CALDWELL, M. M. Solar uv irradiation and the growth and development of higher plants. **Photophysiology**, v. 6, p. 131–177, 1971.

CASICCIA, C.; ZAMORANO, F.; HERNANDEZ, A. Erythemal irradiance at the magellan's region and antarctic ozone hole 1999-2005. **Atmosfera**, Centro de Ciencias de la Atmósfera, UNAM, v. 21, n. 1, p. 1–12, 2008.

COARITI, J. R. Características da radiação ultravioleta solar e seus efeitos na saúde humana nas cidades de la paz–bolívia e natal–brasil. Brasil, 2017.

CORREA, M. et al. Changes in the total ozone content over the period 2006 to 2100 and the effects on the erythemal and vitamin d effective uv doses for south america and antarctica. **Photochemical & Photobiological Sciences**, Springer, v. 18, n. 12, p. 2931–2941, 2019.

CORRÊA, M. d. P. Solar ultraviolet radiation: properties, characteristics and amounts observed in brazil and south america. **Anais brasileiros de dermatologia**, SciELO Brasil, v. 90, p. 297–313, 2015.

CORRÊA, M. de P.; PIRES, L. C. Doses of erythemal ultraviolet radiation observed in b razil. **International Journal of Dermatology**, Wiley Online Library, v. 52, n. 8, p. 966–973, 2013.

COULSON, K. Solar and terrestrial radiation-methods and measurements (book review). **Astrophysical Letters**, v. 17, p. 55, 1976.

CPTEC, C. de Previsão de tempo e estudos climáticos Instituto Nacional de P. E. **Thermal infrared channel**. 2017. Disponível em: <http://satelite.cptec.inpe.br/home/index.jsp>.

DAMIANI, A. et al. Cloud cover and uv index estimates in chile from satellite-derived and ground-based data. **Atmospheric Research**, Elsevier, v. 138, p. 139–151, 2014.

DAUBECHIES, I. **Ten lectures on wavelets**. [S.l.]: SIAM, 1992.

DIFFEY, B. Analysis of the risk of skin cancer from sunlight and solaria in subjects living in northern europe. **Photo-dermatology**, v. 4, n. 3, p. 118–126, 1987.

____. Solar ultraviolet radiation effects on biological systems. **Physics in medicine & biology**, IOP Publishing, v. 36, n. 3, p. 299, 1991.

DIJK, A. van et al. The action spectrum for vitamin d3: initial skin reaction and prolonged exposure. **Photochemical & Photobiological Sciences**, Springer, v. 15, n. 7, p. 896–909, 2016.

DOBSON, G. M. B. Origin and distribution of the polyatomic molecules in the atmosphere. **Proceedings of the Royal Society of London. Series A. Mathematical and Physical Sciences**, The Royal Society London, v. 236, n. 1205, p. 187–193, 1956.

DOUGLASS, A. R.; NEWMAN, P. A.; SOLOMON, S. The antarctic ozone hole: An update. American Institute of Physics (AIP), 2014.

ELIAS, A. G.; ARTIGAS, M. Zossi de. A search for an association between the equatorial stratospheric qbo and solar uv irradiance. **Geophysical research letters**, Wiley Online Library, v. 30, n. 16, 2003.

ENGELSEN, O. The relationship between ultraviolet radiation exposure and vitamin d status. **Nutrients**, Molecular Diversity Preservation International, v. 2, n. 5, p. 482–495, 2010.

FARMAN, J. C.; GARDINER, B. G.; SHANKLIN, J. D. Large losses of total ozone in antarctica reveal seasonal clox/nox interaction. **Nature**, Nature Publishing Group, v. 315, n. 6016, p. 207–210, 1985.

FIOLETOV, V.; KERR, J. B.; FERGUSSON, A. The uv index: definition, distribution and factors affecting it. **Canadian journal of public health**, Springer, v. 101, n. 4, p. I5–I9, 2010.

FITZPATRICK, T. B. The validity and practicality of sun-reactive skin types i through vi. **Archives of dermatology**, American Medical Association, v. 124, n. 6, p. 869–871, 1988.

FLURY, T.; WU, D. L.; READ, W. Variability in the speed of the brewer–dobson circulation as observed by aura/mls. **Atmospheric Chemistry and Physics**, Copernicus GmbH, v. 13, n. 9, p. 4563–4575, 2013.

FU, Q. et al. Observed changes in brewer–dobson circulation for 1980–2018. **Environmental Research Letters**, IOP Publishing, v. 14, n. 11, p. 114026, 2019.

GARCÍA-HUIDOBRO, M. R. et al. Seawater-temperature and uv-radiation interaction modifies oxygen consumption, digestive process and growth of an intertidal fish. **Marine environmental research**, Elsevier, v. 129, p. 408–412, 2017.

GIOVANNI, P. **NASA Earth Data**. 2017. Disponível em: <https://https://giovanni.gsfc.nasa.gov/giovanni/>.

GRANT, R. H.; HEISLER, G. M. Estimation of ultraviolet-b irradiance under variable cloud conditions. **Journal of applied meteorology**, v. 39, n. 6, p. 904–916, 2000.

GRANT, W. B. et al. Evidence that vitamin d supplementation could reduce risk of influenza and covid-19 infections and deaths. **Nutrients**, Multidisciplinary Digital Publishing Institute, v. 12, n. 4, p. 988, 2020.

GROSS, B. et al. Spatio-temporal propagation of covid-19 pandemics. **EPL (Europhysics Letters)**, IOP Publishing, v. 131, n. 5, p. 58003, 2020.

GUARNIERI, R. A. et al. Ozone and uv-b radiation anticorrelations at fixed solar zenith angles in southern brazil. **Geofísica Internacional**, Universidad Nacional Autónoma de México, v. 43, n. 1, p. 17–22, 2004.

HATHAWAY, D. H. The solar cycle. **Living reviews in solar physics**, Springer, v. 12, n. 1, p. 1–87, 2015.

HERMAN, J. et al. Interannual variability of ozone and uv-b ultraviolet exposure. **Journal of Geophysical Research: Atmospheres**, Wiley Online Library, v. 105, n. D23, p. 29189–29193, 2000.

HOFMANN, D. et al. Ten years of ozonesonde measurements at the south pole: Implications for recovery of springtime antarctic ozone. **Journal of Geophysical Research: Atmospheres**, Wiley Online Library, v. 102, n. D7, p. 8931–8943, 1997.

HOLICK, M. F. Sunlight, uv-radiation, vitamin d and skin cancer: how much sunlight do we need? **Sunlight, vitamin D and skin cancer**, Springer, p. 1–15, 2008.

____. The vitamin d deficiency pandemic: Approaches for diagnosis, treatment and prevention. **Reviews in Endocrine and Metabolic Disorders**, Springer, v. 18, n. 2, p. 153–165, 2017.

HOSKINS, B. J.; MCINTYRE, M. E.; ROBERTSON, A. W. On the use and significance of isentropic potential vorticity maps. **Quarterly Journal of the Royal Meteorological Society**, Wiley Online Library, v. 111, n. 470, p. 877–946, 1985.

HRIBAR, C. A.; COBBOLD, P. H.; CHURCH, F. C. Potential role of vitamin d in the elderly to resist covid-19 and to slow progression of parkinsons disease. **Brain sciences**, Multidisciplinary Digital Publishing Institute, v. 10, n. 5, p. 284, 2020.

IALONGO, I.; CASALE, G.; SIANI, A. Comparison of total ozone and erythemal uv data from omi with ground-based measurements at rome station. **Atmospheric Chemistry and Physics**, Copernicus GmbH, v. 8, n. 12, p. 3283–3289, 2008.

IBGE, I. B. de Geografia e E. **Estudos e análises Informação Demográfica e Socioeconômica n. 2. Características étnico-raciais da população: Classificação e identidades.** 2013. Disponível em: <https://biblioteca.ibge.gov.br/visualizacao/livros/liv63405.pdf>.

ICSU, W. U. U. World meteorological organization. 1999.

ILLUMINATION, I. C. on. **Erythema reference action spectrum and standard erythema dose**. 2019. Disponível em: <https://cie.co.at/publications/erythema-reference-action-spectrum-and-standard-erythema-dose-0>.

JANSEN, M. A.; NOORT, R. E. V. D. Ultraviolet-b radiation induces complex alterations in stomatal behaviour. **Physiologia Plantarum**, Wiley Online Library, v. 110, n. 2, p. 189–194, 2000.

JÚNIOR, R. d. S. N. et al. Effects of the el niño southern oscillation phenomenon and sowing dates on soybean yield and on the occurrence of extreme weather events in southern brazil. **Agricultural and Forest Meteorology**, Elsevier, v. 290, p. 108038, 2020.

KAKANI, V. et al. Field crop responses to ultraviolet-b radiation: a review. **Agricultural and forest meteorology**, Elsevier, v. 120, n. 1-4, p. 191–218, 2003.

KAYANO, M. T.; ANDREOLI, R. V. Relationships between rainfall anomalies over northeastern brazil and the el niño–southern oscillation. **Journal of Geophysical Research: Atmospheres**, Wiley Online Library, v. 111, n. D13, 2006.

KAZADZIS, S. et al. Ozone monitoring instrument spectral uv irradiance products: comparison with ground based measurements at an urban environment. **Atmospheric Chemistry and Physics**, Copernicus GmbH, v. 9, n. 2, p. 585–594, 2009.

KERR, J.; FIOLETOV, V. E. Surface ultraviolet radiation. **Atmosphere-Ocean**, Taylor & Francis, v. 46, n. 1, p. 159–184, 2008.

KIRCHHOFF, V. et al. Evidence for an ozone hole perturbation at 30 south. **Atmospheric Environment**, Elsevier, v. 30, n. 9, p. 1481–1488, 1996.

KIRCHHOFF, V. W. J. H. **Ozônio e Radiação UV-B**. [S.l.]: Transtec, 1995.

KLEISS, J. M. et al. Cloud area distributions of shallow cumuli: A new method for ground-based images. **Atmosphere**, Multidisciplinary Digital Publishing Institute, v. 9, n. 7, p. 258, 2018.

KRZYŚCIN, J. W.; PUCHALSKI, S. Aerosol impact on the surface uv radiation from the ground-based measurements taken at belsk, poland, 1980–1996. **Journal of Geophysical Research: Atmospheres**, Wiley Online Library, v. 103, n. D13, p. 16175–16181, 1998.

LEHMANN, B.; QUERINGS, K.; REICHRATH, J. Vitamin d and skin: new aspects for dermatology. **Experimental dermatology**, Wiley Online Library, v. 13, p. 11–15, 2004.

LINDZEN, R. S.; HOLTON, J. R. A theory of the quasi-biennial oscillation. **Journal of Atmospheric Sciences**, v. 25, n. 6, p. 1095–1107, 1968.

LIOU, K.-N. **An introduction to atmospheric radiation**. [S.l.]: Elsevier, 2002. v. 84.

LIU, S.; MCKEEN, S.; MADRONICH, S. Effect of anthropogenic aerosols on biologically active ultraviolet radiation. **Geophysical Research Letters**, Wiley Online Library, v. 18, n. 12, p. 2265–2268, 1991.

LUIZ, E. W. et al. Comparação de metodologias para a estimativa da fração de cobertura de nuvens utilizando câmera all-sky e satélite. In: **VII Congresso Brasileiro de Energia Solar-CBENS 2018**. [S.l.: s.n.], 2018.

MALLOY, K. D. et al. Solar uvb-induced dna damage and photoenzymatic dna repair in antarctic zooplankton. **Proceedings of the National Academy of Sciences**, National Acad Sciences, v. 94, n. 4, p. 1258–1263, 1997.

MANATSA, D.; MUKWADA, G. A connection from stratospheric ozone to el niño-southern oscillation. **Scientific Reports**, Nature Publishing Group, v. 7, n. 1, p. 1–10, 2017.

MARCHAND, M. et al. Model simulations of the impact of the 2002 antarctic ozone hole on the midlatitudes. **Journal of the atmospheric sciences**, v. 62, n. 3, p. 871–884, 2005.

MCGEE, T. J.; JR, J. B. So2 absorption cross sections in the near uv. **Journal of Quantitative Spectroscopy and Radiative Transfer**, Elsevier, v. 37, n. 2, p. 165–182, 1987.

MCKENZIE, R. et al. Cloud cover measured by satellite and from the ground: Relationship to uv radiation at the surface. **International Journal of Remote Sensing**, Taylor & Francis, v. 19, n. 15, p. 2969–2985, 1998.

METOFFICE. **El Niño, La Niña, and the Southern oscillation**. 2022. Disponível em: <www.metoffice.gov.uk/research/climate/seasonal-to-decadal/gpc-outlooks/el-nino-la-nina/enso-description>.

MOLINA, L.; MOLINA, M. Absolute absorption cross sections of ozone in the 185-to 350-nm wavelength range. **Journal of Geophysical Research: Atmospheres**, Wiley Online Library, v. 91, n. D13, p. 14501–14508, 1986.

MOLINA, M. J.; ROWLAND, F. S. Stratospheric sink for chlorofluoromethanes: chlorine atom-catalysed destruction of ozone. **Nature**, Nature Publishing Group, v. 249, n. 5460, p. 810–812, 1974.

NOZAWA, H. et al. Ground-based observation of solar uv radiation in japan, brazil and chile. **Revista Brasileira de Geofísica**, SciELO Brasil, v. 25, p. 17–25, 2007.

OKE, T. R. **Boundary layer climates**. [S.l.]: Routledge, 2002.

OMI, O. M. I. **OMI Algorithm Theoretical Basis Document Volume III Clouds, Aerosols, and Surface UV Irradiance**. 2002. Disponível em: <https://eospso.gsfc.nasa.gov/sites/default/files/atbd/ATBD-OMI-03.pdf>.

ORGANIZATION, W. H.; CONTROL, R. for I. T. **WHO report on the global tobacco epidemic, 2008: the MPOWER package**. [S.l.]: World Health Organization, 2008.

ORGANIZATION, W. H. et al. Global solar uv index: A practical guide. a joint recommendation of the world health organization. **World Meteorological Organization, United Nations Environment Programme, and the International Commission on Non-Ionizing Radiation Protection**, p. 28, 2002.

PARISI, A. et al. Measured and modelled contributions to uv exposures by the albedo of surfaces in an urban environment. **Theoretical and applied climatology**, Springer, v. 76, n. 3, p. 181–188, 2003.

PARKER, S. **O livro do Corpo humano**. [S.l.]: Ciranda Cultural, 2014.

PARTOSOEBROTO, A. **Ray of light Improving measurements of solar ultraviolet radiation**. 2014. Disponível em: <http://kippzonen-brewer.com/wp-content/uploads/2014/10/Publication-MTI2014-Ray-of-Light-by-KippZonen.pdf>.

PERES, L. V. et al. Measurements of the total ozone column using a brewer spectrophotometer and toms and omi satellite instruments over the southern space observatory in brazil. In: COPERNICUS GMBH. **Annales Geophysicae**. [S.l.], 2017. v. 35, n. 1, p. 25–37.

PERES, L. V. et al. Efeito secundário do buraco de ozônio antártico sobre o sul do brasil. Universidade Federal de Santa Maria, 2013.

PERES, L. V. et al. **Monitoramento da coluna total de ozônio e a ocorrência de eventos de influência do buraco de ozônio antártico sobre o sul do Brasil**. 2016. Tese (Doutorado) — Universidade Federal de Santa Maria, 2016.

____. Long term monitoring and climatology of stratospheric fields when the occurrence of influence of the antarctic ozone hole over south of brazil events. **Revista Brasileira de Meteorologia**, SciELO Brasil, v. 34, p. 151–163, 2019.

PFEIFER, G. P.; BESARATINIA, A. Uv wavelength-dependent dna damage and human non-melanoma and melanoma skin cancer. **Photochemical & photobiological sciences**, Royal Society of Chemistry, v. 11, n. 1, p. 90–97, 2012.

PLUMB, R. A. Stratospheric transport. **Journal of the Meteorological Society of Japan. Ser. II**, Meteorological Society of Japan, v. 80, n. 4B, p. 793–809, 2002.

PORTAFAIX, T. et al. Fine-scale study of a thick stratospheric ozone lamina at the edge of the southern subtropical barrier. **Journal of Geophysical Research: Atmospheres**, Wiley Online Library, v. 108, n. D6, 2003.

PREEZ, D. J. D. et al. Solar ultraviolet radiation in pretoria and its relations to aerosols and tropospheric ozone during the biomass burning season. **Atmosphere**, Multidisciplinary Digital Publishing Institute, v. 12, n. 2, p. 132, 2021.

PREEZ, D. J. du et al. Spring and summer time ozone and solar ultraviolet radiation variations over cape point, south africa. v. 37, n. 2, p. 129–141, 2019.

RAPTIS, I.-P. et al. The combined effect of ozone and aerosols on erythemal irradiance in an extremely low ozone event during may 2020. **Atmosphere**, Multidisciplinary Digital Publishing Institute, v. 12, n. 2, p. 145, 2021.

RASTOGI, A. et al. Short term, high-dose vitamin d supplementation for covid-19 disease: a randomised, placebo-controlled, study (shade study). **Postgraduate medical journal**, The Fellowship of Postgraduate Medicine, v. 98, n. 1156, p. 87–90, 2022.

RHODES, J. M. et al. Perspective: Vitamin d deficiency and covid-19 severity–plausibly linked by latitude, ethnicity, impacts on cytokines, ace2 and thrombosis. **Journal of internal medicine**, Wiley Online Library, v. 289, n. 1, p. 97–115, 2021.

RIGOZO, N. R. et al. Reconstruction and searching ozone data periodicities in southern brazil (29ºs, 53ºw). **Revista Brasileira de Meteorologia**, SciELO Brasil, v. 27, n. 2, p. 243–252, 2012.

ROBINSON, N. **Solar Radiation Elsevier Publishing Company**. [S.l.]: Amsterdam, 1966.

ROLPH, G.; STEIN, A.; STUNDER, B. Real-time environmental applications and display system: Ready. **Environmental Modelling & Software**, Elsevier, v. 95, p. 210–228, 2017.

ROUSSEAUX, M. C. et al. Ozone depletion and uvb radiation: Impact on plant dna damage in southern south america. **Proceedings of the National Academy of Sciences**, National Acad Sciences, v. 96, n. 26, p. 15310–15315, 1999.

ROZEMA, J. et al. Toward solving the uv puzzle. **Science**, American Association for the Advancement of Science, v. 296, n. 5573, p. 1621–1622, 2002.

____. Uv-b as an environmental factor in plant life: stress and regulation. **Trends in ecology & evolution**, Elsevier, v. 12, n. 1, p. 22–28, 1997.

SALBY, M.; CALLAGHAN, P. Connection between the solar cycle and the qbo: The missing link. **Journal of Climate**, American Meteorological Society, v. 13, n. 2, p. 328–338, 2000.

SARRA, A. D. et al. Effects of desert dust and ozone on the ultraviolet irradiance at the mediterranean island of lampedusa during paur ii. **Journal of Geophysical Research: Atmospheres**, Wiley Online Library, v. 107, n. D18, p. PAU–2, 2002.

SCHAFER, J. et al. Observed influence of clouds on ultraviolet-b radiation. **Geophysical research letters**, Wiley Online Library, v. 23, n. 19, p. 2625–2628, 1996.

SCHMUCKI, D. A.; PHILIPONA, R. Uv radiation in the alps: the altitude effect. In: SPIE. **Ultraviolet ground-and space-based measurements, models, and effects**. [S.l.], 2002. v. 4482, p. 234–239.

SCHUCH, A. P. **Avaliação da ação genotóxica induzida pela radiação ultravioleta solar na molécula de DNA**. 2009. 150 p. Tese (Doutorado) — Universidade Federal de Santa Maria, Santa Maria, 2009.

SCHUCH, A. P. et al. Identification of influential events concerning the antarctic ozone hole over southern brazil and the biological effects induced by uvb and uva radiation in an endemic treefrog species. **Ecotoxicology and Environmental Safety**, Elsevier, v. 118, p. 190–198, 2015.

____. Dna damage profiles induced by sunlight at different latitudes. **Environmental and Molecular Mutagenesis**, Wiley Online Library, v. 53, n. 3, p. 198–206, 2012.

SCI-TEC, I. I. **Brewer Ozone Spectrophotometer Operators Manual MKIII167.** 1999. Disponível em: <https://www.kippzonen.com/Product/50/Brewer-MkIII-Spectrophotometer#.Yp5Ex6jMKM8>.

SEINFELD, J.; PANDIS, S. **ATMOSPHERIC From Air Pollution to Climate Change SECOND EDITION (p. 1225). Hoboken**. [S.l.]: New Jersey: Wiley-Interscience, 2006.

SEMANE, N. et al. An unusual stratospheric ozone decrease in the southern hemisphere subtropics linked to isentropic air-mass transport as observed over irene (25.5 s, 28.1 e) in mid-may 2002. **Atmospheric Chemistry and Physics**, Copernicus GmbH, v. 6, n. 7, p. 1927–1936, 2006.

SETLOW, R. B. The wavelengths in sunlight effective in producing skin cancer: a theoretical analysis. **Proceedings of the National Academy of Sciences**, National Acad Sciences, v. 71, n. 9, p. 3363–3366, 1974.

SILVA, I. N. de Câncer José Alencar Gomes da. **Estimativa 2020 Incidência de Câncer no Brasil. Ministério da Saúde.** 2019. Disponível em: <https://www.inca.gov.br/sites/ufu.sti.inca.local/files/media/document/estimativa-2020-incidencia-de-cancer-no-brasil.pdf>.

SLATER, D.; LONG, C.; TOOMAN, T. Total sky imager/whole sky imager cloud fraction comparison. In: **Proc. 11th ARM Science Team Meeting**. [S.l.: s.n.], 2001. p. 1–11.

SMITH, S. M.; OWENS, H. B. Clouds and the earth's radiant energy system. investigating the climate system. problem-based classroom modules. **National Aeronautics and Space Administration (NASA)**, ERIC, 2003.

SOLOMON, S. et al. Emergence of healing in the antarctic ozone layer. **Science**, American Association for the Advancement of Science, v. 353, n. 6296, p. 269–274, 2016.

STANECK, M. **Software for Ozone Spectrophotometers**. 2008. Url-http://www.o3soft.eu/uvbrewer.html.

STULL, R. B.; AHRENS, C. D. et al. **Meteorology for scientists and engineers**. [S.l.]: Brooks/Cole, 2000.

TANSKANEN, A. et al. Surface ultraviolet irradiance from omi. **IEEE transactions on Geoscience and Remote Sensing**, IEEE, v. 44, n. 5, p. 1267–1271, 2006.

TERAMURA, A. H. Effects of ultraviolet-b radiation on the growth and yield of crop plants. **Physiologia Plantarum**, Wiley Online Library, v. 58, n. 3, p. 415–427, 1983.

TIBA, C.; LEAL, S. d. S. Enhancement of uv radiation by cloud effect in ne of brazil. **International Journal of Photoenergy**, Hindawi, v. 2017, 2017.

TORRENCE, C.; COMPO, G. P. A practical guide to wavelet analysis. **Bulletin of the American Meteorological society**, American Meteorological Society, v. 79, n. 1, p. 61–78, 1998.

TROSHICHEV, O.; GABIS, I. Variations of solar uv irradiance related to short-term and medium-term changes of solar activity. **Journal of Geophysical Research: Space Physics**, Wiley Online Library, v. 103, n. A9, p. 20659–20667, 1998.

WANG, F. et al. Risk of eye damage from the wavelength-dependent biologically effective uvb spectrum irradiances. **PLoS One**, Public Library of Science San Francisco, USA, v. 7, n. 12, p. e52259, 2012.

____. The distribution of biologically effective uv spectral irradiances received on a manikin face that cause erythema and skin cancer. **Journal of Photochemistry and Photobiology B: Biology**, Elsevier, v. 140, p. 205–214, 2014.

WEBB, A. R. et al. Airborne measurements of ground and cloud spectral albedos under low aerosol loads. **Journal of Geophysical Research: Atmospheres**, Wiley Online Library, v. 109, n. D20, 2004.

WEIHS, P. et al. Measurements of uv irradiance within the area of one satellite pixel. **Atmospheric Chemistry and Physics**, Copernicus GmbH, v. 8, n. 18, p. 5615–5626, 2008.

WHO. Ultraviolet radiation (environmental health criteria 160). **WHO, Geneva**, 1994.

WOODS, T. N. et al. Validation of the uars solar ultraviolet irradiances: Comparison with the atlas 1 and 2 measurements. **Journal of Geophysical Research: Atmospheres**, Wiley Online Library, v. 101, n. D6, p. 9541–9569, 1996.

ZARATTI, F. et al. Erythemally weighted uv variations at two high-altitude locations. **Journal of Geophysical Research: Atmospheres**, Wiley Online Library, v. 108, n. D9, 2003.

ZHANG, J. et al. Influence of the el niño southern oscillation on the total ozone column and clear-sky ultraviolet radiation over china. **Atmospheric Environment**, Elsevier, v. 120, p. 205–216, 2015.